To the Graduate Council:

I am submitting herewith a thesis written by Trent Lee Nichols entitled "Partial Wave Analysis of the Charge Density Distributions for Impurities in Gold." I recommend that it be accepted in partial fulfillment of the requirements for the degree of Master of Science, with a major in Physics.

Paul G. Huray, Major Professor

We have read this thesis
and recommend its acceptance:

Accepted for the Council:

Vice Chancellor
Graduate Studies and Research

Thesis
78
.N545
cop. 2

# PARTIAL WAVE ANALYSIS OF THE CHARGE DENSITY DISTRIBUTIONS FOR IMPURITIES IN GOLD

A Thesis

Presented for the

Master of Science

Degree

The University of Tennessee, Knoxville

Trent Lee Nichols

December 1978

1373066

Copyright by Trent Lee Nichols 1978
All Rights Reserved

## ACKNOWLEDGMENTS

The author would like to gratefully acknowledge the help, guidance, and encouragement received both as an undergraduate and graduate student from Dr. Paul G. Huray. His lucid explanations of the physical meaning of the physics has added a great deal to the author's insight and understanding of physics. The author would also like to acknowledge Dr. J. O. Thomson, who taught him a great deal about the world of experimental physics and how to acquire the most meaningful information in the most straightforward manner. A good deal of the author's knowledge in the realm of solid state physics was obtained in a course taught by Dr. T. A. Callcott and the time given by Dr. Callcott as a committee member is greatly appreciated. Dr. J. R. Thompson is to be thanked for the many hours spent in informative discussions on physics as well as diverse topics. Dr. Thompson is also very warmly thanked for his introduction of the author and his wife.

The author would like to especially thank his typist, Mrs. Paul Warwick, for the time and understanding involved in the production of this thesis as well as making special efforts to meet the all too near deadlines. Mr. Andy Sprinkle is also warmly thanked for preparing the figures and printing of this thesis in the face of onrushing deadlines.

The author would like to also acknowledge the help and efforts of all those people who aided in his intellectual development and understanding but who are too numerous to name.

There are several people who deserve a very special acknowledgment and a warmly deserved thank you. Mrs. Joseph F. Summers, the author's

mother-in-law, helped immensely by typing some of the more difficult parts of the final draft. The author's parents, Mr. and Mrs. Ted Nichols, have provided a great deal of encouragement, understanding, and aid during the trying times of the preparation of this thesis. A very richly deserved and deeply felt thank you is expressed for the author's wife, Sally. Without the great deal of time and effort that she so willingly gave, the final draft would have been surely delayed. More importantly, without her understanding, patience, and love, the author would have had an immeasurably more difficult task.

## ABSTRACT

A partial wave scattering model is often employed to describe the change in the electronic charge density at a nucleus due to dilute impurities dissolved substitutionally into a pure metal lattice. The model is often based on a combination of s, p, and d square well pseudo-potentials. In such treatments the modification of the wave function due to higher order scattering is assumed to be negligible in comparison to the s, p, and d scattering and is, therefore, neglected. This work examines quantitatively the contribution of s, p, d, and f partial scattered wave functions at neighboring lattice sites integrated over the conduction band and at the Fermi level. The depth of the square wells are allowed to be dependent on both the angular momentum and spin of the scattering partial waves. The contribution due to bound states which may be formed for sufficiently deep wells is also considered. Mössbauer isomer shift data on solid solution gold alloys is examined within the framework of this model. In addition, the gold alloy Mössbauer data is analyzed using s, p, and d wave functions in order to determine whether or not characteristics of the Mössbauer absorption line are reproduced.

TABLE OF CONTENTS


| CHAPTER | PAGE |
|---|---|
| INTRODUCTION | 1 |
| I. THEORY | 3 |
| Square Well Pseudo-potential Model | 3 |
| The Friedel Sum Rule | 22 |
| The Residual Resistivity | 24 |
| The Differential Mössbauer Isomer Shift | 26 |
| II. COMPUTER ANALYSIS | 27 |
| III. RESULTS AND DISCUSSION | 32 |
| Contribution of the f Angular Momentum Wavefunction to the Scattered Charge Density | 32 |
| A Self-consistent Solution | 50 |
| Applicability of the Model | 53 |
| LIST OF REFERENCES | 65 |
| APPENDIXES | 67 |
| APPENDIX I | 68 |
| APPENDIX II | 76 |
| VITA | 79 |

LIST OF TABLES


| TABLE | | PAGE |
|---|---|---|
| I. | First s Electron Bound State Energies . . . . . | 69 |
| II. | Second s Electron Bound State Energies. . . . . | 71 |
| III. | First p Electron Bound State Energies . . . . . | 72 |
| IV. | Second p Electron Bound State Energies. . . . . | 73 |
| V. | First d Electron Bound State Energies . . . . . | 74 |
| VI. | First f Electron Bound State Energies . . . . . | 75 |
| VII. | Gold Alloy Parameters and Calculated Values . . . . . | 77 |
| VIII. | Phase Shifts, Energies, and Charge Densities for the Alloys. . . . . | 78 |

LIST OF FIGURES


| FIGURE | | PAGE |
|---|---|---|
| 1. | Spherically Symmetric Square Well Pseudo-potential, Where $V(\vec{r}) = E_{B,\vec{k}} - E_{A,\vec{k}} + V_S(\vec{r})$. . . . . | 5 |
| 2. | Phase Shifts Versus Well Height . . . . . | 9 |
| 3. | Well Height, $E_{\ell\sigma}$, Versus the Bound State Energy Eigenvalue $E_{b_{\ell\sigma}}$ for s, p, d, and f Angular Momentum States . . . . . | 13 |
| 4. | First s Bound State Charge Densities. . . . . | 16 |
| 5. | Second s Bound State Charge Densities . . . . . | 17 |
| 6. | First p Bound State Charge Densities. . . . . | 18 |
| 7. | Second p Bound State Charge Densities . . . . . | 19 |
| 8. | First d Bound State Charge Densities. . . . . | 20 |
| 9. | First f Bound State Charge Densities. . . . . | 21 |
| 10. | Scattered Charge Density for a -12 e.V. Height Well . . . . | 34 |
| 11. | Integrated Scattered Charge Density for a -12 e.V. Height Well. . . . . | 35 |
| 12. | Scattered Charge Density for a -28 e.V. Height Well . . . . | 36 |
| 13. | Integrated Scattered Charge Density for a -28 e.V. Height Well. . . . . | 37 |
| 14. | Scattered Charge Density for a -48 e.V. Height Well . . . . | 38 |
| 15. | Integrated Scattered Charge Density for a -48 e.V. Height Well. . . . . | 39 |
| 16. | Scattered Charge Density for a -60 e.V. Height Well . . . . | 40 |
| 17. | Integrated Scattered Charge Density for a -60 e.V. Height Well. . . . . | 41 |

FIGURE PAGE

18. Scattered Charge Density for a -72 e.V. Height Well. . . . . 42

19. Integrated Scattered Charge Density for a -72 e.V. Height Well . . . . . 43

20. Scattered Charge Density for a +12 e.V. Height Well. . . . . 44

21. Integrated Scattered Charge Density for a +12 e.V. Height Well . . . . . 45

22. The Average Scattered Charge Density for s Angular Momentum. 55

23. The Average Scattered Charge Density for p Angular Momentum. 56

24. The Average Scattered Charge Density for d Angular Momentum. 57

25. The Average Scattered Charge Density for f Angular Momentum. 58

26. Experimental Spectrum for 1% Vanadium in Gold, Shifted by 1.2 mm/sec Due to Isomer Shift . . . . . 60

27. Generated Spectrum (asterisks) and Fit for 1% Vanadium in Gold . . . . . 61

28. Experimental Spectrum for 1% Manganese in Gold, Shifted by 1.2 mm/sec Due to Isomer Shift . . . . . 62

29. Generated Spectrum (asterisks) and Fit for 1% Manganese in Gold . . . . . 63

# INTRODUCTION

Dilute alloys have been the subject of much interest in the recent past. A thorough understanding of dilute alloy systems may conceivably allow better predictions as to the characteristics of new alloys for technology. Such an understanding may be gained by formulating a theoretical model which is capable of reproducing the characteristics of the dilute alloy system. The model may then be used to project the characteristics of new alloys. This thesis deals with dilute alloys formed by substitutional dissolution of an impurity into a pure metal host.

The model to describe a dilute alloy system dealt with in this thesis was first proposed by Roberts et al.[1] in 1965 and has been refined slightly so that the actual model is the same as that proposed by Huray et al.[2] in 1976. The model is based upon replacing the real potentials in the alloy by spherically symmetric pseudo-potential square wells which depend upon the angular momentum of incident electrons. The impurity atoms will in general have different effective well heights than those of pure metal host atoms, thus presenting a lattice of perturbation potentials to the conduction electrons. The perturbation potentials give rise to a change in the electronic charge distribution at each of the host metal nuclei. The Hamiltonian for the system may be solved by means of a partial wave analysis approach to obtain the electronic charge density distribution functions in terms of their angular momentum character. This approach or variations on it are often used in describing dilute alloy systems; however, it is common

to use only some combination of the s, p, and/or d angular momentum state wave functions arguing that higher order angular momentum state wave functions would make a negligible contribution to the total electronic charge density distributions. This work endeavors to show the validity of that assumption by considering the contribution of the f angular momentum wave function in comparison to the electronic charge density due to each of the first three (s, p, and d) angular momentum wave functions.

The change in electronic charge density at alloy nuclei is exhibited in the Mössbauer isomer shift. Used in conjunction with the Friedel sum rule and the residual resistivity, a self consistent solution may be found for the well heights required by the proposed model. This analysis has been previously performed for several gold alloys.[3] Here the model has been extended by solving for these well heights to parameterize the square well pseudo-potentials and then using the associated electronic charge density distribution to generate an absorption line based upon configurations of neighboring scattering sites to Mössbauer nuclei. The ability of the model to reproduce the differential Mössbauer isomer shift and to reproduce the absorption line characteristics, such as asymmetry, will give some measure as to quality of the model.

# CHAPTER I

# THEORY

## I. SQUARE WELL PSEUDO-POTENTIAL MODEL

A dilute alloy formed by dissolving impurity atoms substitutionally into a pure metal host may be described by a set of square well pseudo-potentials[1-3]. This is accomplished by modeling the real potential at a host lattice site by a spherically symmetric square well (muffin-tin) pseudo-potential which extends to one-half the nearest neighbor distance. In the alloy a potential $V_A(\vec{r}-\vec{r}_j)$ is taken to exist within a sphere located at host metal sites $\vec{r}_j$ and a potential $V_A(\vec{r}-\vec{r}_m) + \Delta V(\vec{r}-\vec{r}_m)$ is taken to exist within a sphere at impurity sites $\vec{r}_m$ where $\Delta V(\vec{r}-\vec{r}_m)$ is a perturbation potential. This perturbation potential is approximately given by

$$\Delta V(\vec{r}-\vec{r}_m) \cong V_B(\vec{r}-\vec{r}_m) - V_A(\vec{r}-\vec{r}_m) + V_S(\vec{r}-\vec{r}_m)$$

where $V_B(\vec{r}-\vec{r}_m)$ is the potential that the impurity would exhibit as a pure metal itself and $V_S(\vec{r}-\vec{r}_m)$ accounts for screening effects. The Hamiltonian for the alloy is then[1]

$$\left\{ -\frac{\hbar^2}{2m}\nabla^2 + \sum_{j,\ \text{all atoms}} V_A(\vec{r}-\vec{r}_j) + \sum_{m,\ \text{B atoms}} \Delta V(\vec{r}-\vec{r}_m) \right\} |\vec{k}\rangle_{\text{alloy}} = E_{\vec{k}} |\vec{k}\rangle_{\text{alloy}} \qquad \text{I-1}$$

where the Bloch like pseudo-wave function may be defined as

$$|\vec{k}\rangle_{alloy} = \begin{cases} U_{A,\vec{k}}(\vec{r}-\vec{r}_j)\Phi_{\vec{k}}(\vec{r})/\sqrt{\Omega_A} \text{ at pure metal sites} \\ U_{A,\vec{k}}(a)\Phi_{\vec{k}}(\vec{r})/\sqrt{\Omega_A} \text{ in the interstices between muffin-tins} \\ U_{B,\vec{k}}(\vec{r}-\vec{r}_m)\dfrac{U_{A,\vec{k}}(a)}{U_{B,\vec{k}}(a)}\Phi_{\vec{k}}(r)/\sqrt{\Omega_A} \text{ at impurity sites} \end{cases} \quad \text{I-2}$$

where the Bloch functions, $U_{A,\vec{k}}$ and $U_{B,\vec{k}}$, exhibit the periodicity of the lattice and $\Omega_A$ is the Wigner-Sietz volume for the host. Hence, the function $\phi_{\vec{k}}(r)$ must satisfy

$$\nabla^2\Phi(\vec{r}) + k^2\Phi_{\vec{k}}(\vec{r}) = \begin{cases} \dfrac{2m}{\hbar^2}[E_{B,\vec{k}} - E_{A,\vec{k}} + V_S(\vec{r}-\vec{r}_m)\Phi_k(\vec{r}) \\ \quad \text{for } \vec{r} \text{ in } \vec{r}_m + \vec{a} = U(\vec{r})\Phi_{\vec{k}}(\vec{r}) \\ 0 \\ \quad \text{for } |\vec{r}| \text{ not in } |\vec{r}_m| + \vec{a}. \end{cases} \quad \text{I-3}$$

The potential term on the right hand side is modeled by a spherically symmetric square well pseudo-potential of radius a equal to one-half the nearest neighbor distance. The height of the wells is variable and may depend upon the angular momentum and spin of the conduction electrons relative to the impurity lattice site $\vec{r}_m$, so the potential may be written as

$$U(\vec{r}) = \frac{2m}{\hbar^2}\sum_{\ell=0}^{\infty}\sum_{m=-\ell}^{+\ell}\sum_{\sigma=\uparrow}^{\downarrow} V_{\ell m\sigma}(\vec{r}) = \frac{2m}{\hbar^2}\sum_{\ell=0}^{\infty}\sum_{m=-\ell}^{+\ell}\sum_{\sigma=\uparrow}^{\downarrow}\begin{cases} E_{\ell m\sigma} & |\vec{r}| < a \\ 0 & |\vec{r}| > a \end{cases}$$

(see Figure 1). In all cases it has been assumed that $E_{\ell m\sigma}$ is the same

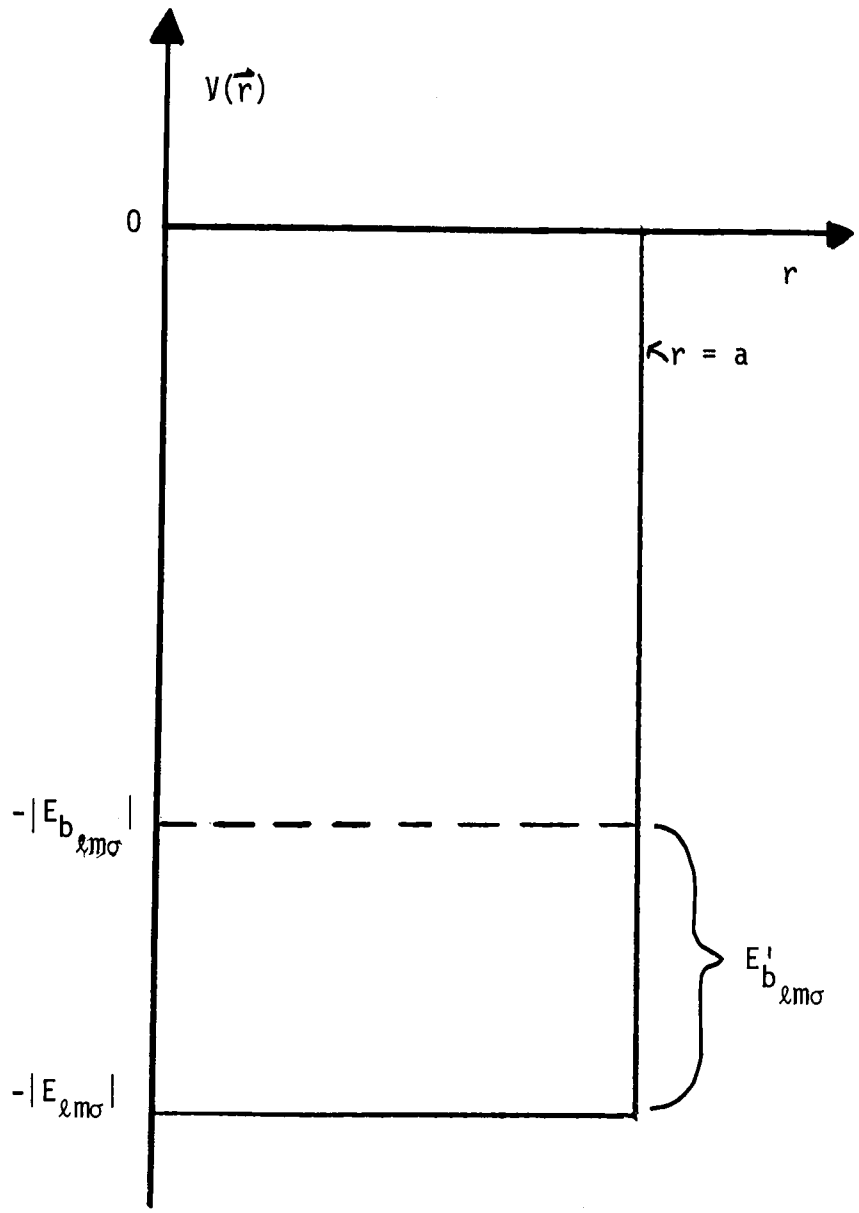


Figure 1. Spherically Symmetric Square Well Pseudo-potential, Where $V(\vec{r}) = E_{B,\vec{k}} - E_{A,\vec{k}} + V_S(\vec{r})$.

for all values of m and often $\sum_{m=-\ell}^{+\ell} E_{\ell m\sigma}$ is replaced by $(2\ell+1)E_{\ell m\sigma}$. In Figure 1 the pseudo-potential is shown as if it were attractive and hence $E_{\ell m\sigma}$ is negative. Using this notation Equation I-3 may be written as

$$\nabla^2 \Phi_{\vec{k}}(\vec{r}) + k'^2_{\ell m\sigma} \Phi_{\vec{k}}(\vec{r}) = 0 \qquad \text{I-4}$$

$$k'^2_{\ell m\sigma} \begin{cases} k^2 - \frac{2m}{\hbar^2} E_{\ell m\sigma} & |\vec{r}| < a \\ k^2 & |\vec{r}| > a. \end{cases}$$

Writing the Laplacian operator $\nabla^2$ in spherical coordinates and using the separation of variables technique the solution may be found to be in the standard form

$$\Phi_{\vec{k}}(\vec{r}) = \sum_{\ell=0}^{\infty} \sum_{m=-\ell}^{+\ell} \sum_{\sigma=\uparrow}^{\downarrow} \begin{Bmatrix} j_\ell(k'_{\ell m\sigma} r) \\ n_\ell(k'_{\ell m\sigma} r) \end{Bmatrix} Y_\ell^m(\theta,\phi)\hat{\sigma} \qquad \text{I-5}$$

if we require that the boundary conditions:

1. $\Phi(r,\theta,\phi) = \Phi(r,\theta,\phi + 2\pi)$
2. $\Phi(r,0,\phi)$ = finite
3. $\Phi(r,\pi,\phi)$ = finite

be satisfied by the solution. The bracket { } in I-5 indicates that a linear combination of the two functions is to be formed with appropriate coefficients to meet further boundary conditions. The pseudo-wave function $\Phi_{\vec{k}}(\vec{r})$ has been constructed (Equation I-2) so that it is

continuous across the spherical boundary at r = a and hence we further require that:

4. $\lim_{\varepsilon\to 0} \Phi(a - \varepsilon,\theta,\phi) = \lim_{\varepsilon\to 0} \Phi(a + \varepsilon,\theta,\phi)$

5. $\lim_{\varepsilon\to 0} \frac{d\phi}{dr}(a - \varepsilon,\theta,\phi) = \lim_{\varepsilon\to 0} \frac{d\phi}{dr}(a + \varepsilon,\theta,\phi)$

6. $\int_0^{2\pi}\int_0^{\pi}\int_0^{\infty} \Phi_b^* \Phi_b r^2 \sin\theta \, dr \, d\theta \, d\phi = 1$

where Condition 6 is the normalization integral for the bound state wave functions. In addition, two implicit boundary conditions exist:

7. $\Phi(0,\theta,\phi)$ = finite

8. $\lim_{r\to\infty} \Phi(r,\theta,\phi)$ = finite.

The form of the solution then depends upon the relative sizes of $k^2$ and $\frac{2m}{\hbar^2} E_{\ell m\sigma}$.

A. If, for example, $\frac{2m}{\hbar^2} E_{\ell m\sigma}$ is repulsive (positive) but $k^2$ is smaller, $\frac{2m}{\hbar^2} E_{\ell m\sigma} > k^2 > 0$ and $k'_{\ell m\sigma}$ is imaginary (see I-4). In this case the solution may be written

$$\Phi_{\vec{k}}(\vec{r}) = \sum_{\ell=0}^{\infty} \sum_{\sigma=\uparrow}^{\downarrow} \frac{e^{i\delta_{\ell\sigma}(k)} i^{\ell}}{i_{\ell}(k'_{\ell\sigma}a)} (2\ell+1) [\cos\delta_{\ell\sigma}(k) j_{\ell}(ka) \qquad \text{I-6}$$

$$- \sin\delta_{\ell\sigma}(k) n_{\ell}(ka)] i_{\ell}(k'_{\ell\sigma}r) P_{\ell}(\cos\theta)\hat{\sigma} \qquad |\vec{r}| < a$$

$$\Phi_{\vec{k}}(\vec{r}) = \sum_{\ell=0}^{\infty} \sum_{\sigma=\uparrow}^{\downarrow} e^{i\delta_{\ell\sigma}(k)} i^{\ell} (2\ell+1) [\cos\delta_{\ell\sigma}(k) j_{\ell}(kr)$$

$$- \sin\delta_{\ell\sigma}(k) n_{\ell}(kr)] \cdot P_{\ell}(\cos\gamma)\hat{\sigma} \qquad |\vec{r}| > a,$$

and the m has been dropped from the subscripts since all potentials are assumed to be m independent. The addition theorem for spherical harmonics has been employed,

$$P_\ell(\cos\gamma) = \frac{4\pi}{2\ell+1} \sum_{m=-\ell}^{+\ell} Y_\ell^{m*}(\theta',\phi) Y_\ell^m(\theta,\phi).$$

The $\delta(k)$ is called the phase shift and from Boundary Conditions 4 and 5, it is required to satisfy (see also Figure 2)

$$\tan\delta_{\ell\sigma}(k) = \frac{ki_\ell(k'_{\ell\sigma}a)j'_\ell(ka) - k'_{\ell\sigma}i'_\ell(k'_{\ell\sigma}a)j_\ell(ka)}{ki_\ell(k'_{\ell\sigma}a)n'_\ell(ka) - k'_{\ell\sigma}i'_\ell(k'_{\ell\sigma}a)n_\ell(ka)}. \qquad \text{I-7}$$

B. If, for example, $\frac{2m}{\hbar^2}E_{\ell m\sigma}$ is repulsive (positive) but $k^2$ is larger, $k^2 > \frac{2m}{\hbar^2}E_{\ell m\sigma} > 0$ and $k'_{\ell m\sigma}$ is real (see I-4). Hence the solution may be written

$$\Phi_{\vec{k}}(\vec{r}) = \sum_{\ell=0}^{\infty} \sum_{\sigma=\uparrow}^{\downarrow} \frac{e^{i\delta_{\ell\sigma}(k)}}{j_\ell(k'_{\ell\sigma}a)} i^\ell(2\ell+1)[\cos\delta_{\ell\sigma}(k)j_\ell(ka)$$

$$- \sin\delta_{\ell\sigma}(k)n_\ell(ka)] \cdot j_\ell(k'_{\ell\sigma}r)P_\ell(\cos\gamma)\hat{\sigma} \qquad |\vec{r}| < a$$

$$\Phi_{\vec{k}}(\vec{r}) = \text{same as above for A} \qquad |\vec{r}| > a.$$

Again the m has been dropped from the subscripts since all potentials are assumed to be m independent. The phase shifts, $\delta_{\ell\sigma}(k)$, are required to satisfy

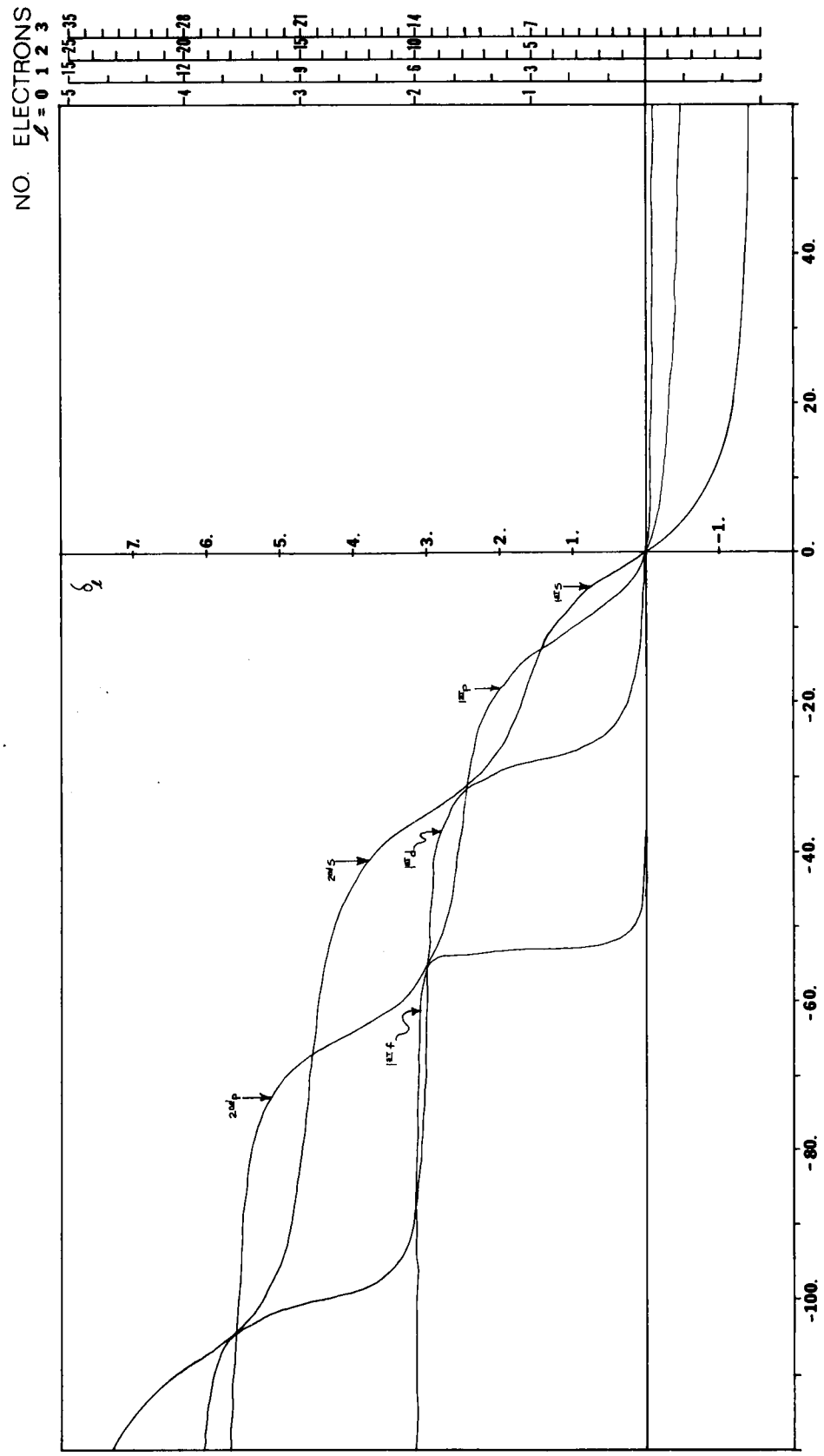


Figure 2. Phase Shifts Versus Well Height.

$$\tan \delta_{\ell\sigma}(k) = \frac{k j_\ell(k'_{\ell\sigma}a) j'_\ell(ka) - k'_{\ell\sigma} j'_\ell(k'_{\ell\sigma}a) j_\ell(ka)}{k j_\ell(k'_{\ell\sigma}a) n'_\ell(ka) - k'_{\ell\sigma} j'_\ell(k'_{\ell\sigma}a) n_\ell(ka)}. \qquad \text{I-8}$$

C. If, for example, $\frac{2m}{\hbar^2} E_{\ell m\sigma}$ is attractive (negative) then $k^2 > 0 > \frac{2m}{\hbar^2} E_{\ell m\sigma}$ and $k'_{\ell m\sigma}$ is real. In this case the solution may be written as in the case of I-8. However, if one of the $E_{b_{\ell m\sigma}}$ is attractive enough, a "bound state" may occur. That is, the Schrödinger Equation I-3 may have a negative value $E_{b_{\ell m\sigma}}$ (see Figure 1) such that

$$\nabla^2 \Phi_b(\vec{r}) + \frac{2m}{\hbar^2} E_{b_{\ell m\sigma}} \Phi_b(\vec{r}) = U(\vec{r}) \Phi_b(\vec{r}) = \frac{2m}{\hbar^2} \begin{cases} E_{\ell m\sigma} & |\vec{r}| < a \\ 0 & |\vec{r}| > a \end{cases} \Phi_b(\vec{r}) \qquad \text{I-9}$$

or defining

$$k'^2_{\ell m\sigma} = \begin{cases} k'^2_{b_{\ell m\sigma}} = \frac{2m}{\hbar^2}(E_{b_{\ell m\sigma}} - E_{\ell m\sigma}) = \frac{2m}{\hbar^2} E'_{b_{\ell m\sigma}} & |\vec{r}| < a \\ k^2_{b_{\ell m\sigma}} = \frac{2m}{\hbar^2} E_{b_{\ell m\sigma}} & |\vec{r}| > a \end{cases}$$

Equation I-4 is again produced with a subscript b. In this case, however, $k'_{b_{\ell m\sigma}}$ is real ($|\vec{r}| < a$) and $k_{b_{\ell m\sigma}}$ is imaginary ($|\vec{r}| > a$). For $|\vec{r}| < a$ Boundary Condition 7 requires that the coefficients of $n_\ell(kr)$ be zero. For $|\vec{r}| > a$ the solution may be expressed in terms of modified spherical Hankel functions of the first and third kind, $i_\ell(k_b r)$ and $k_\ell(k_b r)$, respectively. The Boundary Condition 8 requires that all coefficients of the modified spherical Bessel function of the first kind to be zero. $\Phi_{b_{\ell m\sigma}}$ will be continuous across the boundary at $r = a$ and hence satisfy Condition 4 if we choose the coefficients to be of the form

$$\Phi_{b_{\ell m}}(r,\theta,\phi) = \sum_{\ell=0}^{\infty} \sum_{m=-\ell}^{+\ell} \sum_{\sigma=\uparrow}^{\downarrow} \begin{cases} A_{\ell m\sigma} k_\ell(k_{b_\ell} a) j_\ell(k'_{b_\ell} r) Y_\ell^m(\theta,\phi)\hat{\sigma} & |\vec{r}| < a \\ A_{\ell m\sigma} j_\ell(k'_{b_\ell} a) k_\ell(k_{b_\ell} r) Y_\ell^m(\theta,\phi)\hat{\sigma} & |\vec{r}| > a \end{cases} \qquad \text{I-10}$$

Requiring the continuity of the normal derivative (Boundary Condition 5) supplies an important relationship between $E_{b_{\ell m\sigma}}$ and $E_{\ell m\sigma}$. From I-10 it is seen that this requires

$$\sum_\ell \sum_m \sum_\sigma A_{\ell m\sigma} k_\ell(k_{b_{\ell\sigma}} a) \frac{d}{dr} j_\ell(k'_{b_{\ell\sigma}} r)\Big|_{r=a} Y_\ell^m(\theta,\phi)\hat{\sigma}$$

$$= \sum_\ell \sum_m \sum_\sigma A_{\ell m\sigma} j_\ell(k'_{b_{\ell\sigma}} a) \frac{d}{dr} k_\ell(k_{b_{\ell\sigma}} r)\Big|_{r=a} Y_\ell^m(\theta,\phi)\hat{\sigma}.$$

Equating coefficients of the $Y_\ell^m(\theta,\phi)\hat{\sigma}$

$$k_\ell(k_{b_{\ell\sigma}} a) \frac{d}{dr} j_\ell(k'_{b_{\ell\sigma}} r)\Big|_{r=a} = j_\ell(k'_{b_{\ell\sigma}} a) \frac{d}{dr} k(k_{b_{\ell\sigma}} r)\Big|_{r=a},$$

and using the recursion relation

$$\frac{d}{dx} f_n(x) = \frac{n}{x} f_n(x) - f_n(x)$$

(where $f_n(x)$ may be $k_n(x)$ or $j_n(x)$). Thus, it is seen that

$$k_{b_{\ell\sigma}} \frac{k_{\ell+1}(k_{b_{\ell\sigma}} a)}{k_\ell(k_{b_{\ell\sigma}} a)} = k'_{b_{\ell\sigma}} \frac{j_{\ell+1}(k'_{b_{\ell\sigma}} a)}{j_\ell(k'_{b_{\ell\sigma}} a)}. \qquad \text{I-11}$$

So for a given well depth $E_{\ell m\sigma}$, the bound state energy $E'_{b_{\ell m\sigma}}$ is uniquely determined. Also, by solving the resulting transcendental equation in $E_{\ell m\sigma}$ and $E'_{b_{\ell m\sigma}}$ the point at which binding occurs may be determined. Appendix I contains a set of tables (Tables I through VI) of the bound state energies for wells as deep as 100 e.V. for all s, p, d, and f electrons. When binding occurs, the number of electrons bound is equal to the multiplicity of the state, i.e., $2(2\ell+1)$. Figure 3 is a plot of $E_{b_{\ell m\sigma}}$ versus $E_{\ell m\sigma}$ (the well height).

The constants $A_{\ell m\sigma}$ may be determined by normalizing $\Phi_{b_{\ell m\sigma}}(r,\theta,\phi)$ to one (see Boundary Condition 6)

$$1 = |A_{\ell m\sigma}|^2\{k_\ell^2(k_{b_{\ell m\sigma}}a)\int_0^a j_\ell^2(k'_{b_{\ell m\sigma}}r)r^2dr \qquad \text{I-12}$$

$$+ j_\ell^2(k'_{b_{\ell m\sigma}}a)\int_a^\infty k_\ell^2(k_{b_{\ell m\sigma}}a)r^2dr\}.$$

Carrying out the integration[4] the expression yields

$$A_{\ell m\sigma} = \{\frac{a^3}{2}(j_\ell^2(k'_{b_{\ell m\sigma}}a) - j_{\ell+1}(k'_{b_{\ell m\sigma}}a)j_{\ell-1}(k'_{b_{\ell m\sigma}}a)) \qquad \text{I-13}$$

$$- j_\ell^2(k'_{b_{\ell m\sigma}}a)\frac{a^3}{2}(k_\ell^2(k_{b_{\ell m\sigma}}a) - k_{\ell+1}(k_{b_{\ell m\sigma}}a)k_{\ell-1}(k_{b_{\ell m\sigma}}a))\}^{-1/2}$$

and using the recursion relations

$$\frac{2n+1}{x}k_n(x) = k_{n+1}(x) - k_{n-1}(x)$$

$$\frac{2n+1}{x}j_n(x) = j_{n+1}(x) + j_{n-1}(x)$$

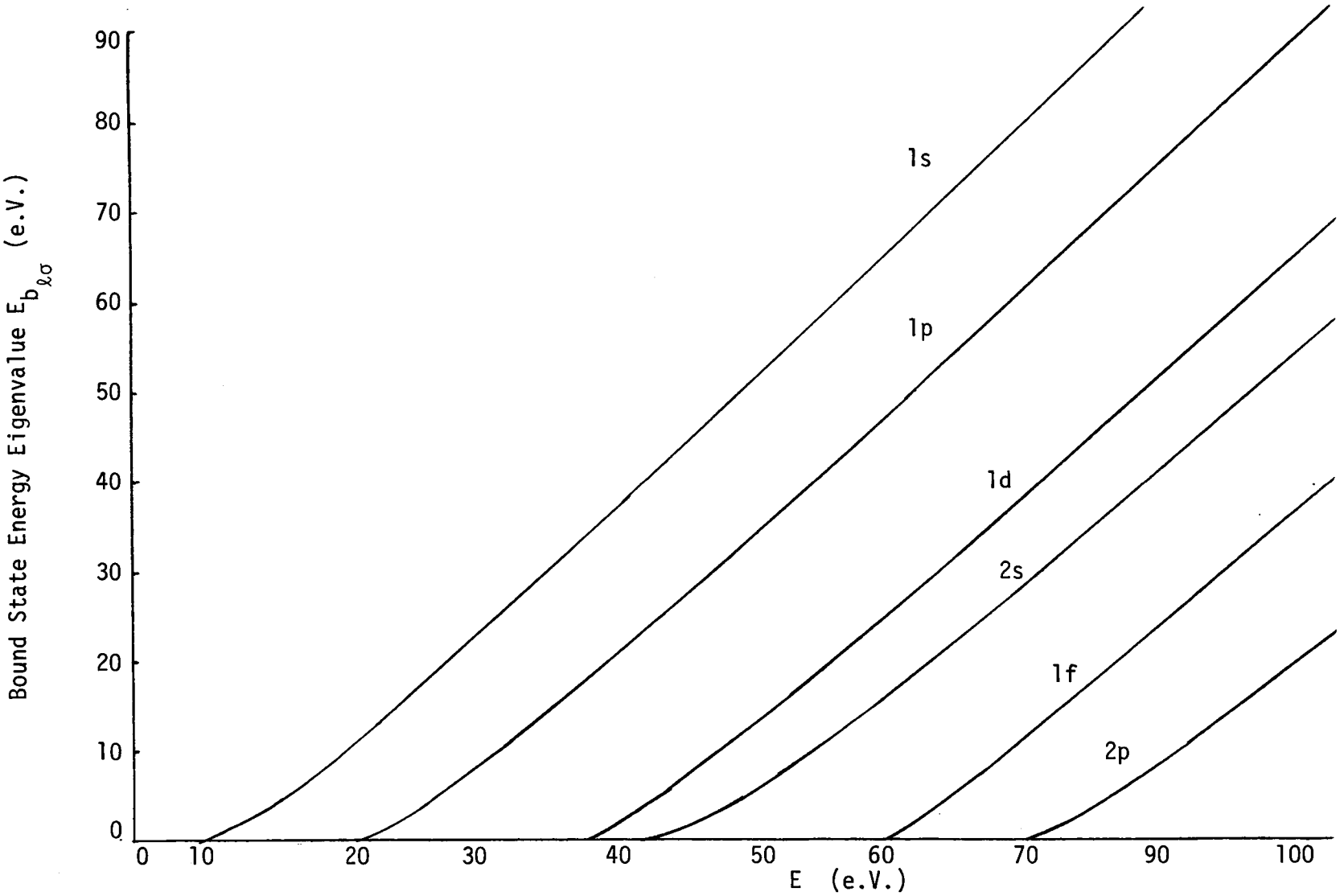


Figure 3. Well Height, $E_{\ell\sigma}$, Versus the Bound State Energy Eigenvalue $E_{b_{\ell\sigma}}$ for s, p, d and f Angular Momentum States.

and Equation I-11 this may be simplified to

$$A_{\ell m\sigma} = \sqrt{\frac{2\,E_{b_{\ell m\sigma}}}{a^3 E_{\ell m\sigma}}}\, k_{\ell+1}(k_{b_{\ell m\sigma}} a) k_{\ell-1}(k_{b_{\ell m\sigma}} a) j_\ell(k'_{b_{\ell m\sigma}} a). \qquad \text{I-14}$$

Hence, the bound state wave functions may be written as follows

$$\Phi_{b_{\ell m\sigma}} = \sqrt{\frac{2\,E'_{b_{\ell m\sigma}}}{a^3 E_{b_{\ell m\sigma}}}}\, \frac{Y_\ell^m(\theta,\phi)}{(k_{\ell+1}(k_{b_{\ell m\sigma}} a) k_{\ell-1}(k_{b_{\ell m\sigma}} a))^{1/2} j_\ell(k_{b_{\ell m\sigma}} a)} \qquad \text{I-15}$$

$$\begin{cases} k_\ell(k_{b_{\ell m\sigma}} a) j_\ell(k_{b_{\ell m\sigma}} r) & |\vec{r}| < a \\ j_\ell(k'_{b_{\ell m\sigma}} a) k_\ell(k_{b_{\ell m\sigma}} r) & |\vec{r}| > a. \end{cases}$$

These functions fall off exponentially outside of the well boundary due to the exponential behavior of the modified spherical Bessel function of the third kind. The fractional bound state charge density at some point r may be obtained by averaging the square of $\Phi_{b_{\ell m\sigma}}$ over $\theta$ and $\phi$. This gives

$$\frac{\langle \Delta\rho_{b_{\ell m\sigma}}(r)\rangle}{\rho_A(0)} = \frac{2\Omega_A E'_{b_{\ell m\sigma}}}{4\pi\, E_{\ell m\sigma}}\, \frac{1}{k_{\ell+1}(k_{b_{\ell\sigma}} a) k_{\ell-1}(k_{b_{\ell\sigma}} a) j_\ell(k_{b_{\ell\sigma}} a)}$$

$$\begin{cases} k^2(k_{b_{\ell\sigma}} a) j^2(k'_{b_{\ell\sigma}} r) & |\vec{r}| < a \\ j_\ell^2(k'_{b_{\ell\sigma}} a) k_\ell^2(k_{b_{\ell\sigma}} r) & |\vec{r}| > a. \end{cases}$$

Figure 4 is a graph of the first s electrons bound state scattered charge density times $r^2a$ versus the radial parameter r/a. It may be seen that the charge tends to be localized predominantly within the well with peak near $r/a \sim 0.6$ for very negative well heights but for less negative well heights the peak is less sharp and much closer to the well boundary. Also, as the well height becomes more negative the amount of charge outside the well boundary is greatly diminished. However, for any height the charge character outside the well is seen to have an exponential character and hence would only contribute a significant amount of charge to the first near neighbors and then only for well heights slightly more negative than the bound state well heights. The second set of s electrons to be bound have two peaks within the well (due to the zeroes of the spherical Bessel function), as is shown in Figure 5. Similarly, Figures 6 through 9 typify the bound state charge distributions for the first and second p, first d, and first f angular momentum states. In all cases the exponential behavior outside the well boundary may be observed. These tendencies are consistent with the definition of bound state, that is, a localized wave function and therefore a localized charge distribution.

The contribution of the fractional bound state charge density (Equation I-16) adds to the previously obtained fractional scattered charge density (Equation I-8). The result is

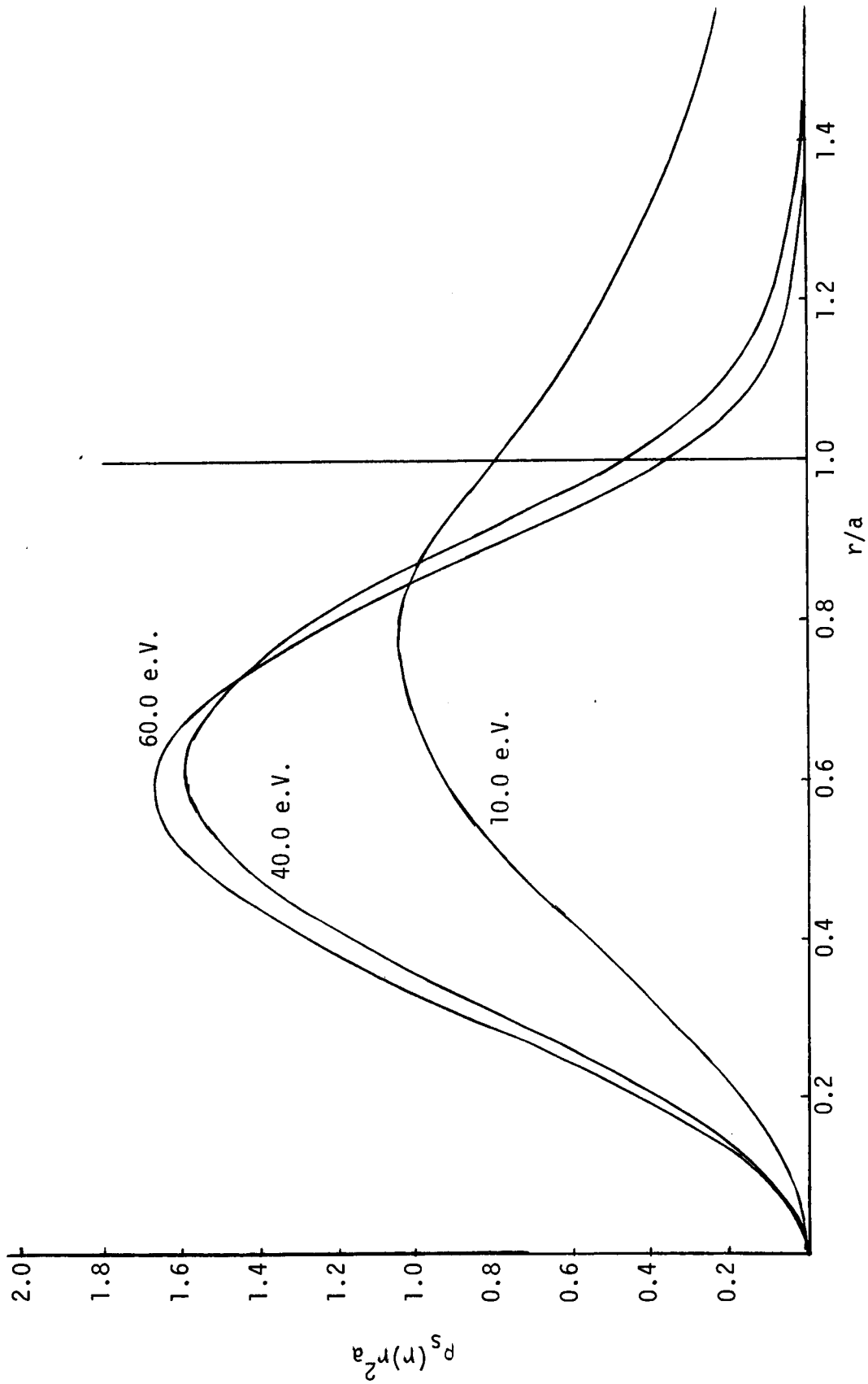


Figure 4. First s Bound State Charge Densities.

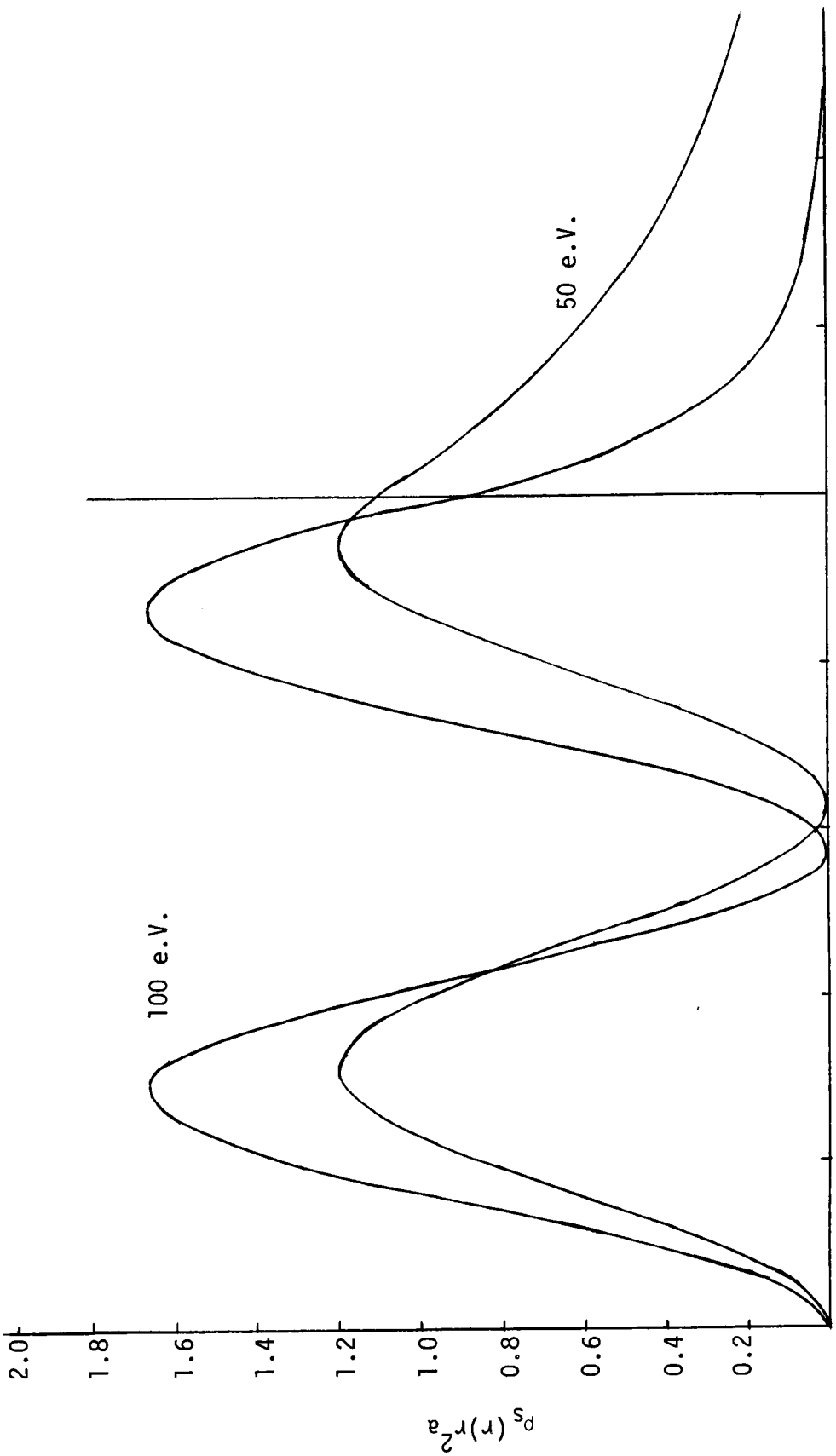


Figure 5. Second s Bound State Charge Densities.

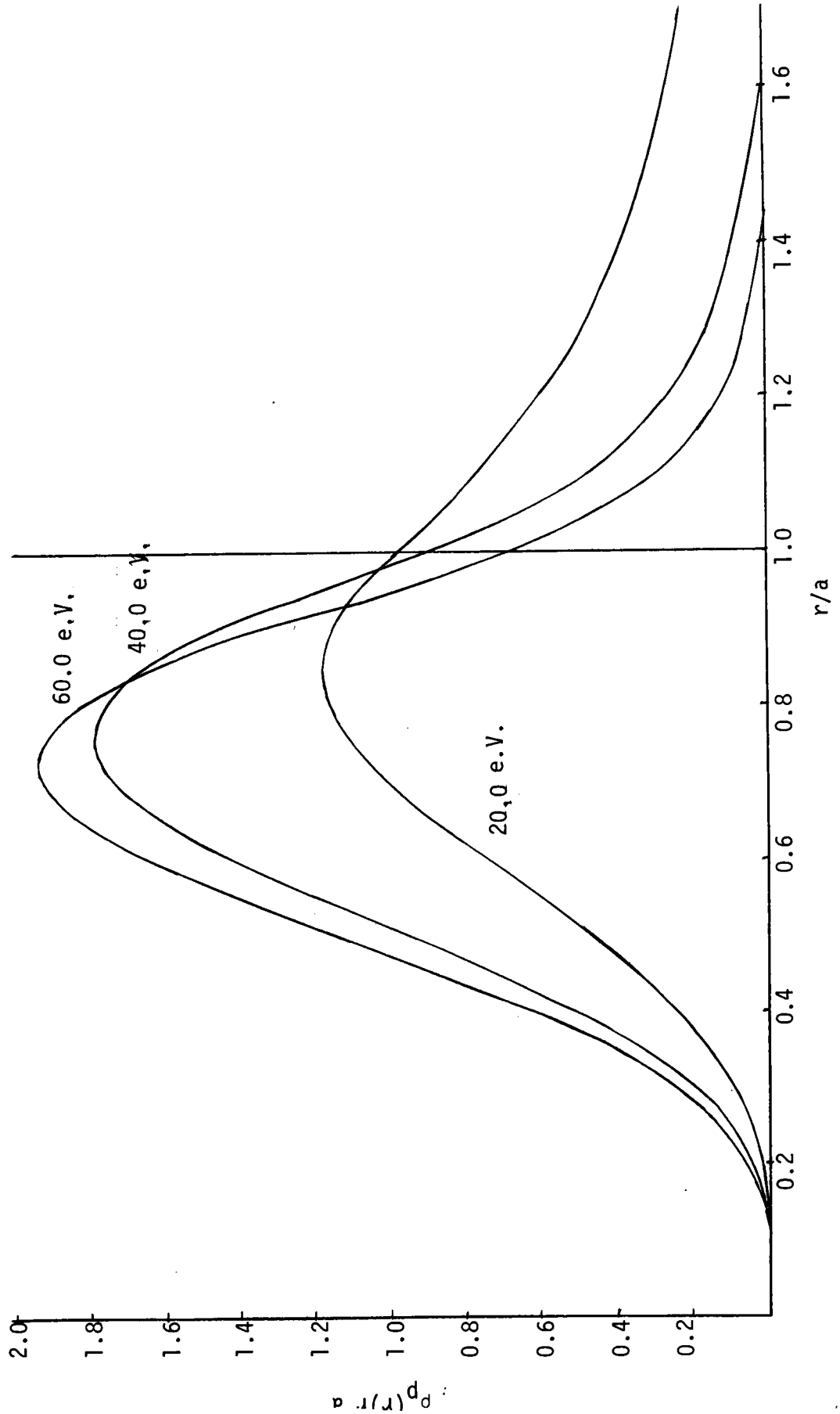


Figure 6. First p Bound State Charge Densities.

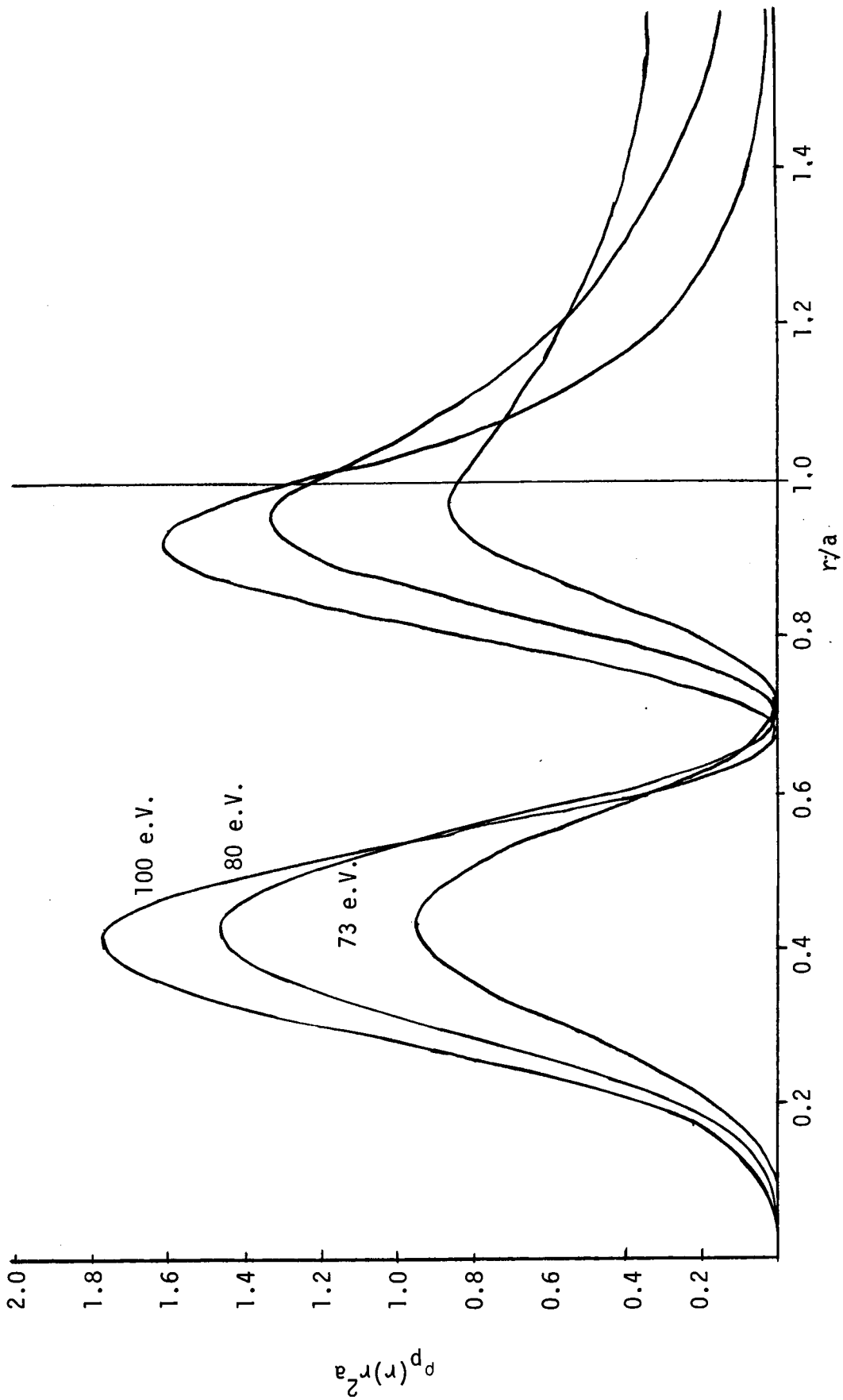


Figure 7. Second p Bound State Charge Densities.

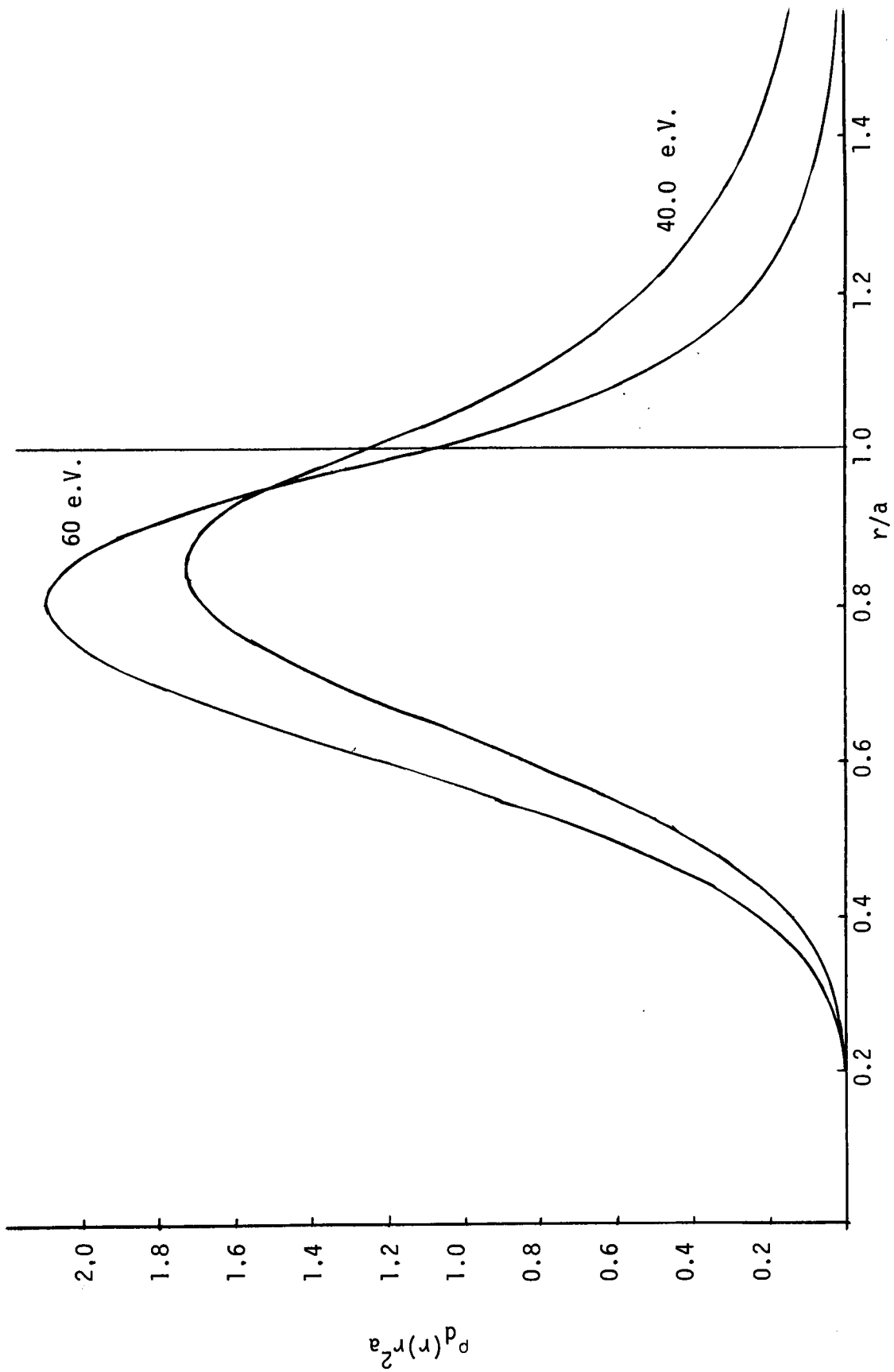


Figure 8. First d Bound State Charge Densities.

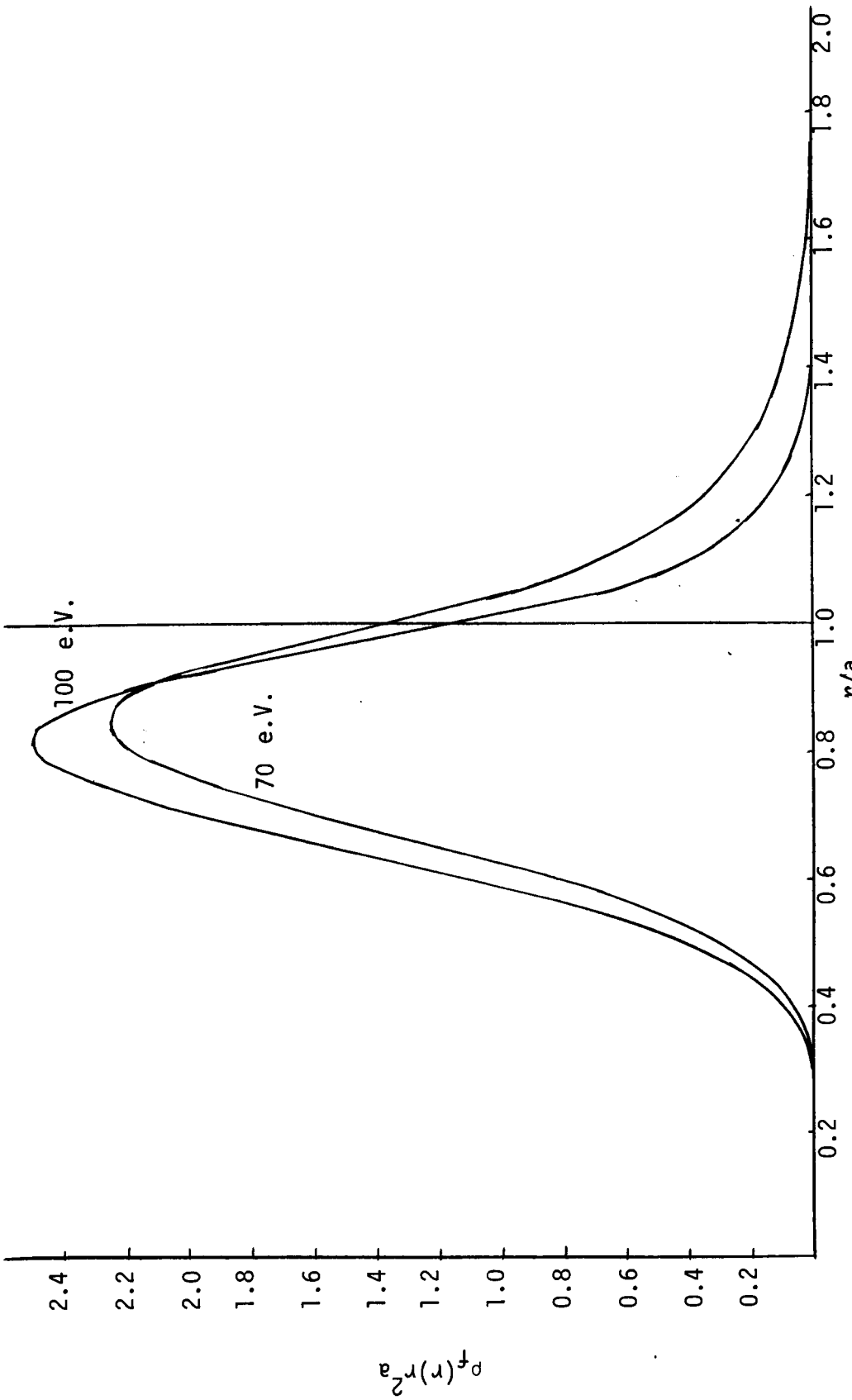


Figure 9. First f Bound State Charge Densities.

$$\frac{\langle \Delta\rho_{sc}(r)\rangle}{\rho_A(0)} = \Omega_A \sum_{\ell}\sum_{\sigma}\left[\frac{2\ell+1}{4\pi}\frac{2}{\pi}\int_0^{k_F}\left\{(\sin\delta_{\ell\sigma}(k)n_\ell(ka)-\cos\delta_{\ell\sigma}(k)j_\ell(ka))^2\right.\right. \quad \text{I-17a}$$

$$\left.\left.\begin{cases} i_\ell^2(k'_{\ell\sigma}r)/i_\ell^2(k'_{\ell\sigma}a), & k^2 < \frac{2m}{\hbar^2}E_{\ell\sigma} \\ j_\ell^2(k'_{\ell\sigma}r)/j_\ell^2(k'_{\ell\sigma}a), & k^2 > \frac{2m}{\hbar^2}E_{\ell\sigma} \end{cases} - j_\ell^2(kr)\right\}k^2dk \quad |\vec{r}| < a\right.$$

$$\left. + \frac{2\ell+1}{4\pi}\frac{2}{a^3}\frac{E'_{b_{\ell\sigma}}}{E_{\ell\sigma}}\frac{k_\ell(k_{b_{\ell\sigma}}a)j_\ell(k'_{b_{\ell\sigma}}r)}{k_{\ell+1}(k_{b_{\ell\sigma}}a)k_{\ell-1}(k_{b_{\ell\sigma}}a)j_\ell(k'_{b_{\ell\sigma}}a)}\right]$$

$$\frac{\langle \Delta\rho_{sc}(r)\rangle}{\rho_A(0)} = \Omega_A \sum_{\ell}\sum_{\sigma}\left[\frac{2\ell+1}{4\pi}\frac{2}{\pi}\int_0^{k_F}\left\{(\sin\delta_{\ell\sigma}(k)n_\ell(kr)-\cos\delta_{\ell\sigma}(k)j_\ell(kr))^2\right.\right. \quad \text{I-17b}$$

$$\left.\left. - j_\ell^2(kr)\right\}k^2dk\right.$$

$$\left.\frac{2\ell+1}{4\pi}\frac{2}{a^3}\frac{E'_{b_{\ell\sigma}}}{E_{\ell\sigma}}\frac{j_\ell(k'_{b_{\ell\sigma}}a)k_\ell(k_{b_{\ell\sigma}}r)}{(k_{\ell+1}(k_{b_{\ell\sigma}}a)k_{\ell-1}(k_{b_{\ell\sigma}}a)j_\ell(k'_{b_{\ell\sigma}}a))}\right] |\vec{r}| > a.$$

The sum over m has been carried out in I-17. Since wells are assumed to be of the same depth for all values of m, the sum over m has been replaced by $(2\ell+1)$ and all m subscripts have been dropped.

## II. THE FRIEDEL SUM RULE

An electron which is scattered by the spherically symmetric pseudo-potentials previously described possesses an angularly averaged charge density distribution of the form of Equation I-17. Integration over the conduction band to a large radius R, that is

$$N = \int_0^R \langle \Delta\rho_{sc}(r) \rangle \, 4\pi r^2 dr$$

produces the Friedel sum rule given by[5]

$$N = \frac{1}{\pi} \sum_{\ell,\sigma} (2\ell+1)\delta_{\ell,\sigma}(k_F) + N_{bound} \qquad \text{I-18}$$

where an additive oscillatory term has been omitted since it is comparatively small at large distances in the lattice. This expression gives the number of extra electrons in the neighborhood of a scattering potential required to neutralize or "screen" its charge, thus ensuring the charge neutrality of the sample. The electrons due to bound states, $N_{bound}$, is determined by the multiplicity of the state times the number of states bound.

In an unaltered lattice, N may be taken to be the nominal valence difference of the free atom host and the impurity, $\Delta Z$. However, the addition of an impurity normally distorts the lattice which in turn gives rise to an effective change in the charge density of the solid. This modification of $\Delta Z$ is given by[1,6]

$$N = \Delta Z - \frac{1-\sigma'}{1+\sigma'} \frac{\delta a}{a}$$

where $\sigma'$ is the Poisson ratio and $\delta a/a$ is the differential change in lattice parameter due to a one atomic percent impurity.

The phase shifts are taken to be independent of spin by many authors (i.e., $\delta_{1\uparrow} = \delta_{1\downarrow}$). However, for magnetic alloys it is often

desirable to take $\delta_2 = \frac{1}{2}(\delta_{2\uparrow} + \delta_{2\downarrow})$. In this case, the spin of the impurity may be given as[3]

$$S = \frac{1}{2}(N_\uparrow - N_\downarrow) = \frac{1}{2\pi}\sum_{\ell}(2\ell+1)(\delta_{\ell\sigma}(k_F) - \delta_{\ell\sigma}(k_F)) \qquad \text{I-20}$$

and if only d electrons are assumed to contribute to the spin density oscillations

$$S = \frac{5}{2\pi}(\delta_{2\uparrow} - \delta_{2\downarrow}).$$

## III. THE RESIDUAL RESISTIVITY

In an alloy the resistivity is composed of two terms, one due to the thermal motion of the lattice and the other due to the scattering of the conduction electrons by impurity potentials. For dilute alloys, the latter term is called the residual resistivity. The residual resistivity may be found by extrapolating the resistivity curve to 0°K since the lattice contribution to the resistivity vanishes at that point.

The residual resistivity may also be found by expressing the wave function $\Phi_{\vec{k}}(\vec{r})$ of Equation I-6 in terms of a Legendre expansion of the form

$$\Phi_{\vec{k}}(\vec{r}) = e^{ik\cdot r} + f(\theta)\frac{e^{ikr}}{r} \qquad \text{I-21}$$

$$= \sum_{\ell=\sigma}^{\infty}\sum_{\sigma=\uparrow}^{\downarrow}(2\ell+1)i^{\ell}e^{i\delta_{\ell\sigma}(k)}\frac{1}{kr}\sin(kr - \tfrac{1}{2}\ell\pi + \delta_{\ell\sigma}(k))P_{\ell}(\cos(\theta))\hat{\sigma}.$$

Here the asymptotic forms of $j_\ell(kr)$ and $n_\ell(kr)$ have been used. The differential scattering cross-section, $\Sigma(\theta)$, may be found by expanding $\exp(i\vec{k}\cdot\vec{r})$ in terms of Legendre polynomials. The result is

$$\Sigma(\theta) = |f(\theta)|^2 = \frac{1}{k^2} \sum_{\ell=0}^{\infty} \sum_{\sigma=\uparrow}^{\downarrow} (2\ell+1) e^{i\delta_{\ell\sigma}(k)} \sin \delta_{\ell\sigma}(k) P_\ell(\cos\theta)\hat{\sigma}. \qquad \text{I-22}$$

The resistivity for n carriers per unit volume and p impurities per unit volume may be shown to be[7]

$$\frac{1}{\sigma} = \frac{p\hbar k_F}{ne^2} \langle \Sigma(\theta) \rangle. \qquad \text{I-23}$$

Hence the residual resistivity is found to be[7]

$$\frac{1}{\sigma} = \frac{2\pi\hbar p}{ne^2 k_F} \sum_{\ell=0}^{\infty} \sum_{\sigma=\downarrow}^{\uparrow} (\ell+1) \sin^2 (\delta_{\ell,\sigma}(k_F) - \delta_{\ell+1,\sigma}(k_F)) \qquad \text{I-24}$$

where the phase shifts are evaluated at the Fermi level since only electrons at the Fermi level can contribute to the resistivity. It is often convenient to express the ratio p/n in terms of the atomic fraction of impurities m. This relation may be shown to be $m(1-m) = p/n$ so the residual resistivity is then

$$\frac{1}{\sigma} = \frac{2\pi\hbar m(1-m)}{e^2 k_F} \sum_{\ell=0}^{\infty} \sum_{\sigma=\uparrow}^{\downarrow} (\ell+1) \sin^2(\delta_{\ell,\sigma}(k_F) - \delta_{\ell+1,\sigma}(k_F)). \qquad \text{I-25}$$

# IV. THE DIFFERENTIAL MÖSSBAUER ISOMER SHIFT

The differential Mössbauer isomer shift is the difference between the isomer shift for Mössbauer nuclei in the dilute alloy and the pure metal. The isomer shift is found to depend upon the average alloy volume and the composition. An approximate theoretical model for the differential isomer shift taking into account these effects has been proposed by Huray et al.[2] In the context of the pseudo-potential model, this differential isomer shift is found to be[2]

$$\delta(\Delta E) = kn\rho_A(0)\left\{\left(\frac{\Omega_A}{\Omega_{alloy}}\right)^{\gamma}\left(1 + m\sum_i c_i \frac{<\Delta\rho_{sc}(r_i)>}{\Omega_A(0)} - 1\right)\right\} \qquad \text{I-26}$$

where $\Omega_A$ and $\Omega_{alloy}$ are the atomic values of the pure metal and alloy, respectively. $\gamma$ is a constant which may be determined theoretically to have a value of $\sim$0.86, the number of atoms in the $i^{th}$ shell of nearest neighbors is denoted by $c_i$, the average scattered charge density, $<\Delta\rho_{sc}(r_i)>/\rho_A(0)$, may be determined by evaluating Equation I-17b at the radius $r_i$ of the $i^{th}$ set of neighbors. The coefficient $kn\rho_A(0)$ has been previously determined by Roberts et al.[1] to have the value of $\sim$8.0 mm/sec. The term involving the summations is the total fractional scattered charge density brought about at the pure metal nuclei located at $\vec{r}_i$ due to the screening cloud of electrons associated with the impurity located at $r = 0$.

# CHAPTER II

## COMPUTER ANALYSIS

Computer analysis of the problem is accomplished primarily by four routines, three of which are computer codes and the fourth is a hand calculator code. The computer codes are: CHRGDN (an acronymm for charge density), LORENT (an acronym for Lorentzian line), and SPDWEL (an acronym for s, p, and d well depth). The routines CHRGDN and LORENT are designed to execute as batch programs on an IBM 360 model 65 computer and to utilize a CalComp pen plotter and associated software; the routine SPDWEL operates in a time sharing mode on a DEC System-10 computer. All computations were performed at the University of Tennessee Computing Center (UTCC) which operates all of the aforementioned hardware and software. The card images of codes CHRGDN and LORENT reside on disk data sets on the Dec System-10 where they may be easily edited and submitted directly to the IBM 360 model 65. The fourth routine is written for a Hewlett-Packard model 67 (HP 67) hand calculator on magnetic cards.

The bound state well heights are found for a particular well height by the routine designed to execute on the HP 67. A transcendental equation (I-11) given in the theory section is solved by the routine and the root yields the bound state energy eigenvalue. The program has as its inputs the angular momentum quantum number, the well heights in electron volts (here a positive number is an attractive well), and a guess at the root of the transcendental equation in terms of $k'_{b_\sigma} a$.

SPDWEL is designed to calculate the potential well height which corresponds to the input phase shift at the Fermi level and to the input angular momentum quantum number. The routine solves a transcendental equation given in Chapter I (Equations I-7 and I-8) by a Newton-Rhapson method.[8]

The routine CHRGDN was originally written only for s, p, and d angular momentum states but was rewritten to include the f angular momentum state, to calculate the Mössbauer isomer shift, and to plot the Knight shift, the fractional scattered charge density and the total scattered charge density. Well heights in electron volts for the s, p, d, and f potential wells, a differential lattice parameter change, bound state energies (if applicable), and a title are input parameters to the routine. Flags are used to select what calculations are to be performed. The fractional scattered charge densities require an integration over the conduction band, i.e., from $k = 0$ to $k = k_F$. These integrations are performed by a standard five point Gauss-Legendre integration technique.[8] However, since the interval in k-space over the conduction band is large, the integral may be broken into several sub-integrals thus providing a better approximation. Subroutines have been coded to calculate the first five spherical Bessel, spherical Neumann, spherical McDonald and modified spherical Bessel functions. The values are calculated by utilizing recursion relations in terms of the elementary functions: sine, cosine, and exponential. In the case of small arguments of the spherical Bessel or spherical Neumann functions a series expansion is used to avoid roundoff errors.

The Lorentzian line program, LORENT, reads input parameters from catalogued disk data sets produced by CHRGDN. Each of the neighboring atoms contribute to the charge density at the origin, that is, at the Mössbauer nucleus. So for the pure metal case an unshifted symmetric Lorentzian line (correcting for any isomer shift due to the gamma ray source) is exhibited. However, if there are neighboring impurities the change in charge density at the Mossbauer nucleus will effect a change in the line shape. The line may be observed to shift and to broaden and possibly to display an asymmetry. The Lorentzian line produced by the Mössbauer nucleus is dependent upon the different configurations that the neighboring impurities may assume. The resultant absorption line is given by

$$\langle I(v)\rangle = \sum_{k_1=0}^{c_1}\sum_{k_2=0}^{c_2}\sum_{k_3}^{c_3}\cdots P_{k_1}P_{k_2}P_{k_3}\cdots \frac{I_0}{[(v-(v_{k_1}+v_{k_2}+v_{k_3}+\ldots))^2+W_0^2/4]} \qquad \text{II-1}$$

where $I_0$ is an arbitrary constant intensity, $W_0$ is the natural line width for an infinitesimally thin absorber, $v_{k_j}$ is the velocity shift caused by k impurities in the $j^{th}$ shell, and $P_{k_1}P_{k_2}P_{k_3}\ldots$ is the probability of occurence of the configuration with $k_i$ impurities in the first shell of $c_1$ sites, $k_2$ impurities in the second shell of $c_2$ sites, and so forth. The assumption is made in calculating the probabilities above that a particular configuration in a particular shell is not affected by the configurations of other shells. The shift of Equation II-1 is given by

$$v_{k_j} = k_j g \frac{\Delta\rho(r_j)}{\rho_A(0)}\text{total} \qquad \text{II-2}$$

where $k_j g$ provides the appropriate conversion into velocity units and $\frac{\Delta\rho(r_j)}{\rho_A(0)}$total is the total fractional scattered charge density from an impurity in the $j^{th}$ shell given in Equations I-17a and I-17b.

If N is used to denote the total number of locations in the p shells under consideration and the number of impurities to be placed in the lattice, then n is equal to N multiplied by the impurity concentration. Now n impurities may be distributed among the N neighboring sites M ways where M is given by

$$M = N(N-1)(N-2)(N-3) \ldots (N-n+1) = \frac{N!}{(n-n)!}. \qquad \text{II-3}$$

If $k_j$ of the n impurities are to be in the $j^{th}$ shell of atoms, the number of configurations that will produce those $k_j$ impurities is given by

$$M = (c_j(c_j-1)(c_j-2)(c_j-3) \ldots (c_j-k_j+1))$$

$$\times ((N-c_j)(N-c_j-1)(N-c_j-2) \ldots (N-c_j-n+k_j+1))$$

$$= \frac{c_j!(N-c_j)!}{(c_j-k_j)!(N-c_j-n+k_j)!}$$

for the case in which the $k_j$ impurities are put into the $j^{th}$ shell first and the remainder are placed elsewhere later. However, the $k_j$ impurities need not go into the $j^{th}$ shell first; any combination of n impurities which has $k_j$ impurities in the $j^{th}$ shell is acceptable. In general there are n!/(n-k)! ways in which to place $k_j$ of the n impurities into

the $j^{th}$ shell. So the probability of a configuration with $k_j$ impurities in the $j^{th}$ shell is given by

$$P_{k_j} = \frac{n!c_j!(N-n)!(n-c_j)!}{N!(c_j-k_j)!(n-k_j)!(N+k_j-c_j-n)!} \cdot \qquad \text{II-5}$$

It will be shown in Chapter III that the first few shells of neighbors contribute most to the charge density change at the origin, so that in evaluating the absorption line by means of the results from CHRGDN only a few sums are taken in Equation II-1. The resulting absorption line exhibits broadening and asymmetry as is displayed in the experimental data. The resulting absorption is then fit to a symmetric broadened Lorentzian line by a standard gradient search technique which minimizes the chi-square test of convergence.[9] A one line fit is used to measure the asymmetry and line broadening. This analysis compares to our experimental analysis in which real asymmetric broadened absorption lines were fit to a symmetric broadened Lorentzian line.

# CHAPTER III

## RESULTS AND DISCUSSION

### I. CONTRIBUTION OF THE f ANGULAR MOMENTUM WAVEFUNCTION TO THE SCATTERED CHARGE DENSITY

It is commonly assumed in the partial wave analysis method that only some combination of the first three angular momentum states (s, p, and d) needs to be included in order to accurately describe the screening cloud associated with impurity atoms in a dilute alloy. There are several reasons for making this assumption. One reason is that incomplete shells of f electrons are not found in the periodic table in free atoms until the rare earths when looking in terms of ascending atomic numbers. Thus, only for rare earth or actinide impurities would f angular momentum states be expected to occur in significant numbers for metals or alloys. Also, due to the higher angular momentum possessed by the f electrons, conduction electrons would be expected classically to scatter significantly into this state only from wells with a large radius. Since the linear momentum of conduction electrons is $\hbar k$ at most and the maximum extent of a scattering is usually thought of in terms of fractions of the Wigner-Seitz radius of the impurity atom, the high angular momentum of the f electrons and the comparatively small extent of the well provides for a classically low probability of f type scattering of conduction electrons.

Since a large body of data exists on dilute gold alloys,[3,10] pure metal conduction band parameters were used to evaluate the contribution of the f angular momentum state to the scattered charge density. The well radius and Fermi level used are found in Appendix II, Table VII. The pseudo-potential model and computer codes constructed are general and hence are applicable to a variety of other alloys.

In order to examine the f contribution for electrons scattered from a gold conduction band (up to about 5 e.V.), test cases of scattering well heights from -80.0 e.V. to +40.0 e.V. were evaluated by the CHRGDN program. The angularly averaged fractional scattered charge density distributions (SCDD) have been calculated and plotted as a function of radius (the origin of coordinates has been taken to be the center of the perturbation potential). The total average charge density at some radius r is obtained by adding together the s, p, d, and f fractional SCDD. The charge within a sphere of radius R may thus be obtained by integrating the s, p, d, and f fractional SCDD out to R. As R is allowed to approach infinity, the integrated SCDD should asymptotically approach the total charge predicted by the Friedel sum rule. Hence, by examining the fractional and integrated scattered charge density distribution plots it is possible to determine the relative contributions to the charge density of the s, p, d, and f angular momentum state wave functions.

Figures 10 through 21 are typical plots of alternately the fractional and integrated SCDD for various well heights. In each case shown here all four wells are taken to have the same height to allow for easier comparison. In all of the figures the first vertical line from

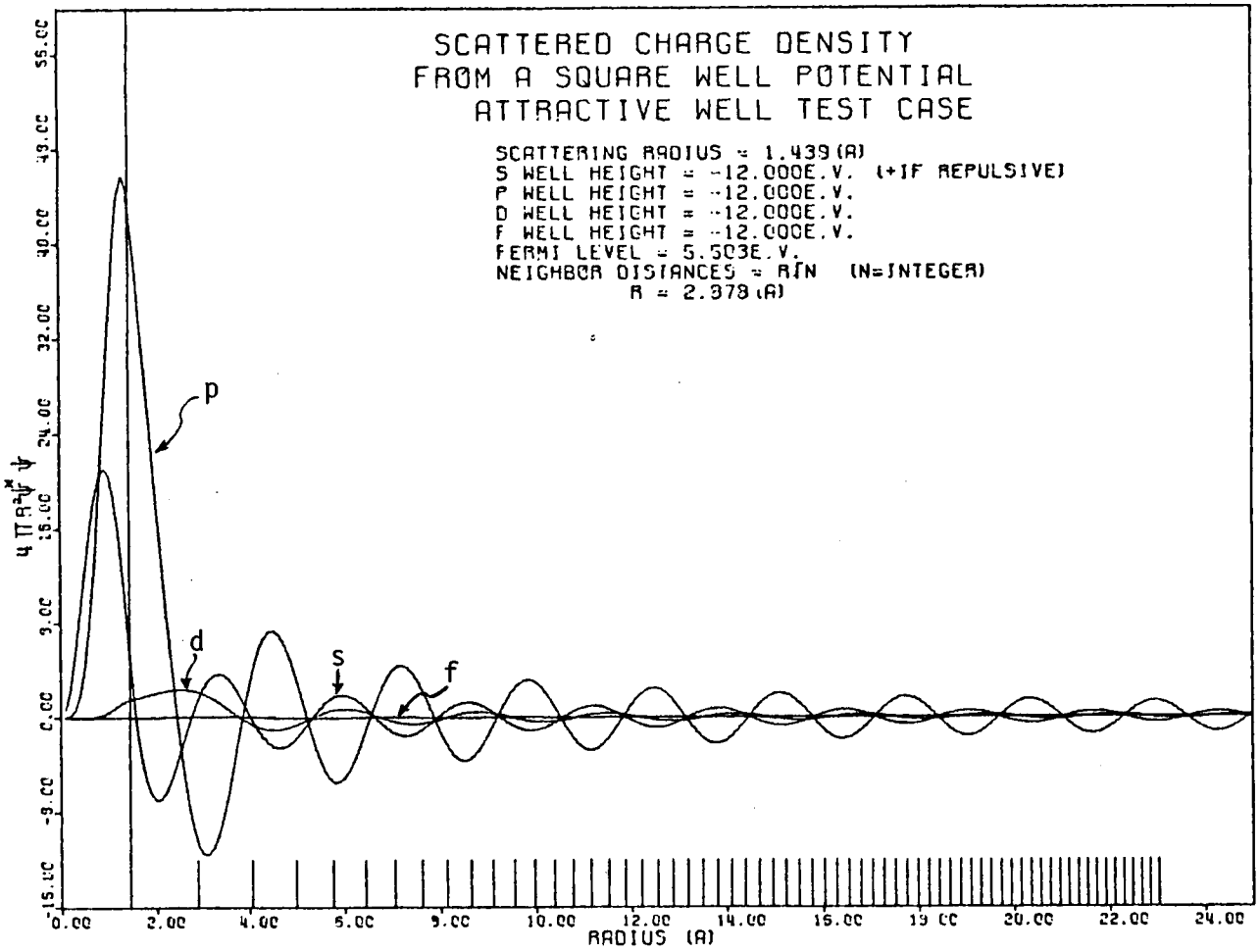


Figure 10. Scattered Charge Density for a -12 e.V. Height Well.

The first vertical line corresponds to the well boundary and the short vertical lines correspond to the position of the first 64 neighbor shells.

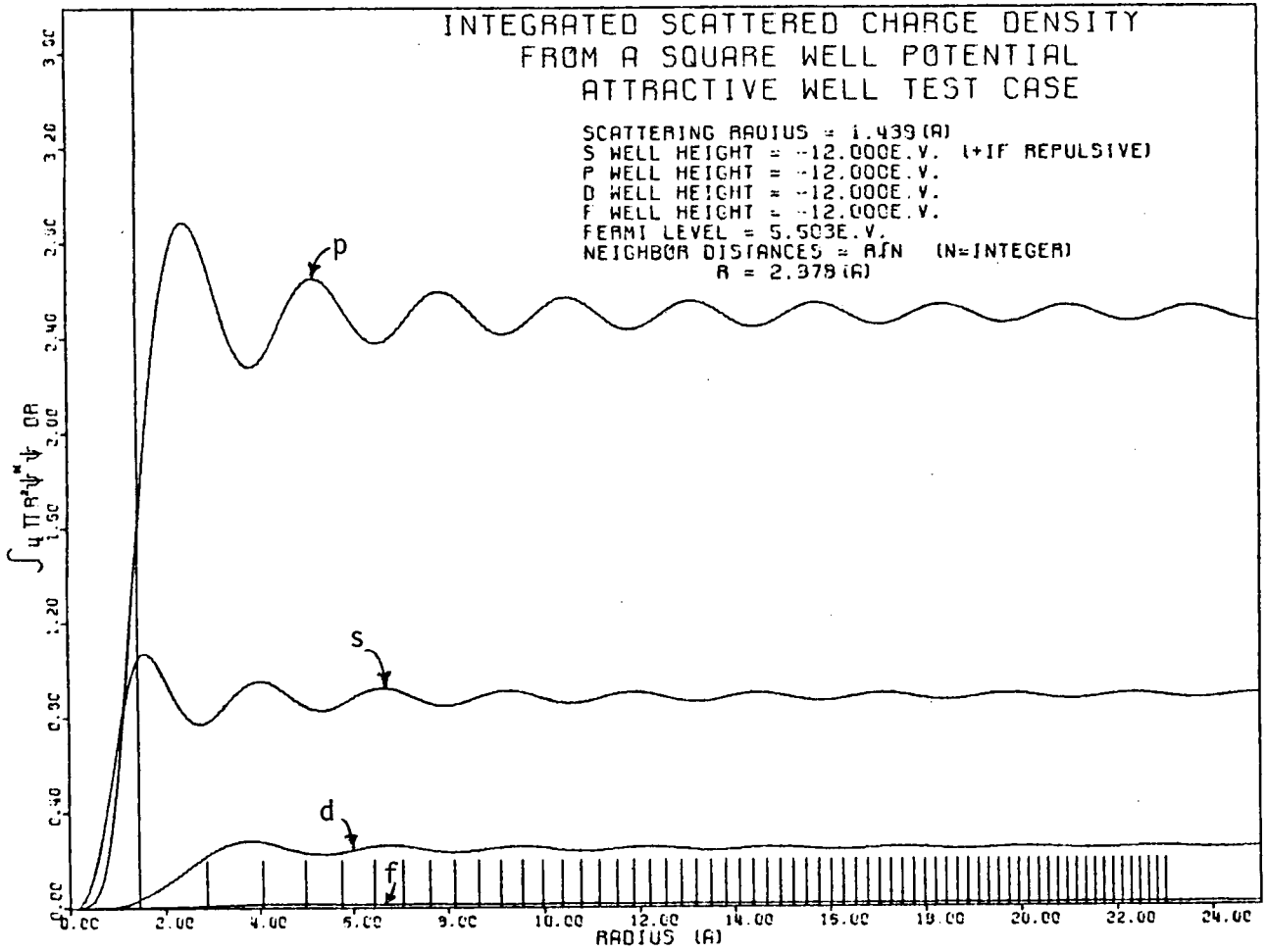


Figure 11. Integrated Scattered Charge Density for a -12 e.V. Height Well.

The first vertical line corresponds to the well boundary and the short vertical lines correspond to the position of the first 64 neighbor shells.

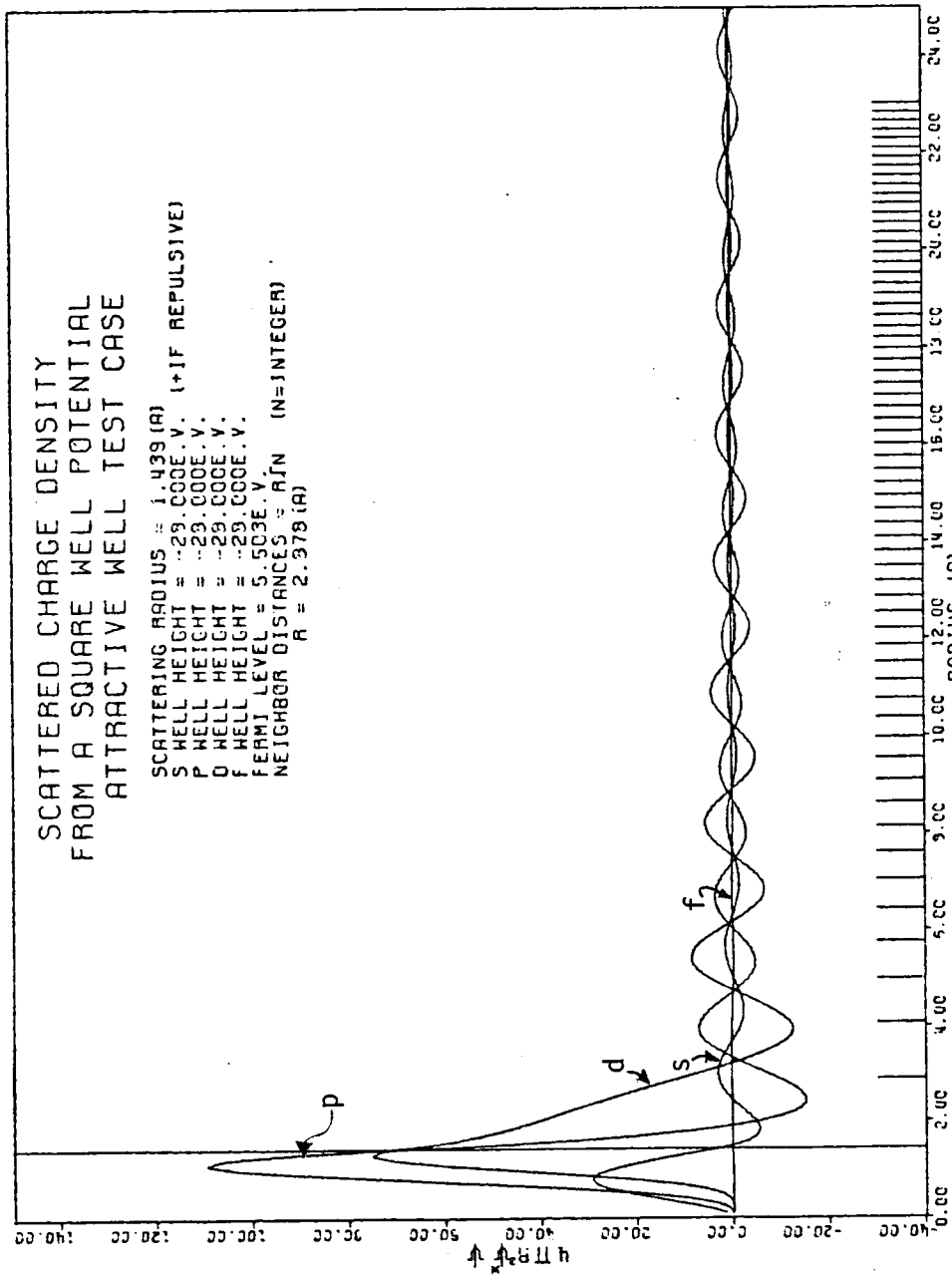


Figure 12. Scattered Charge Density for a -28 e.V. Height Well.

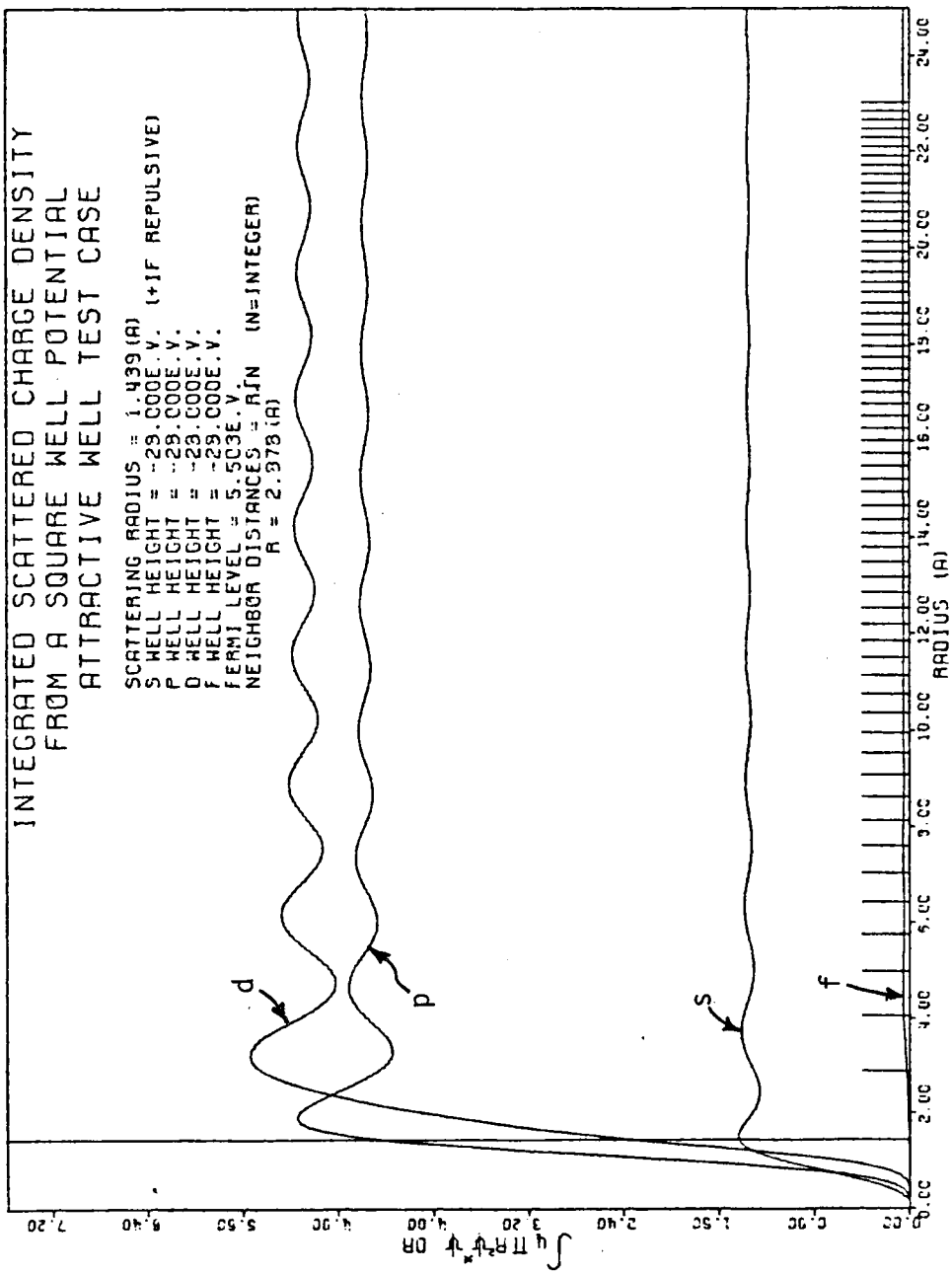


Figure 13. Integrated Scattered Charge Density for a -28 e.V. Height Well.

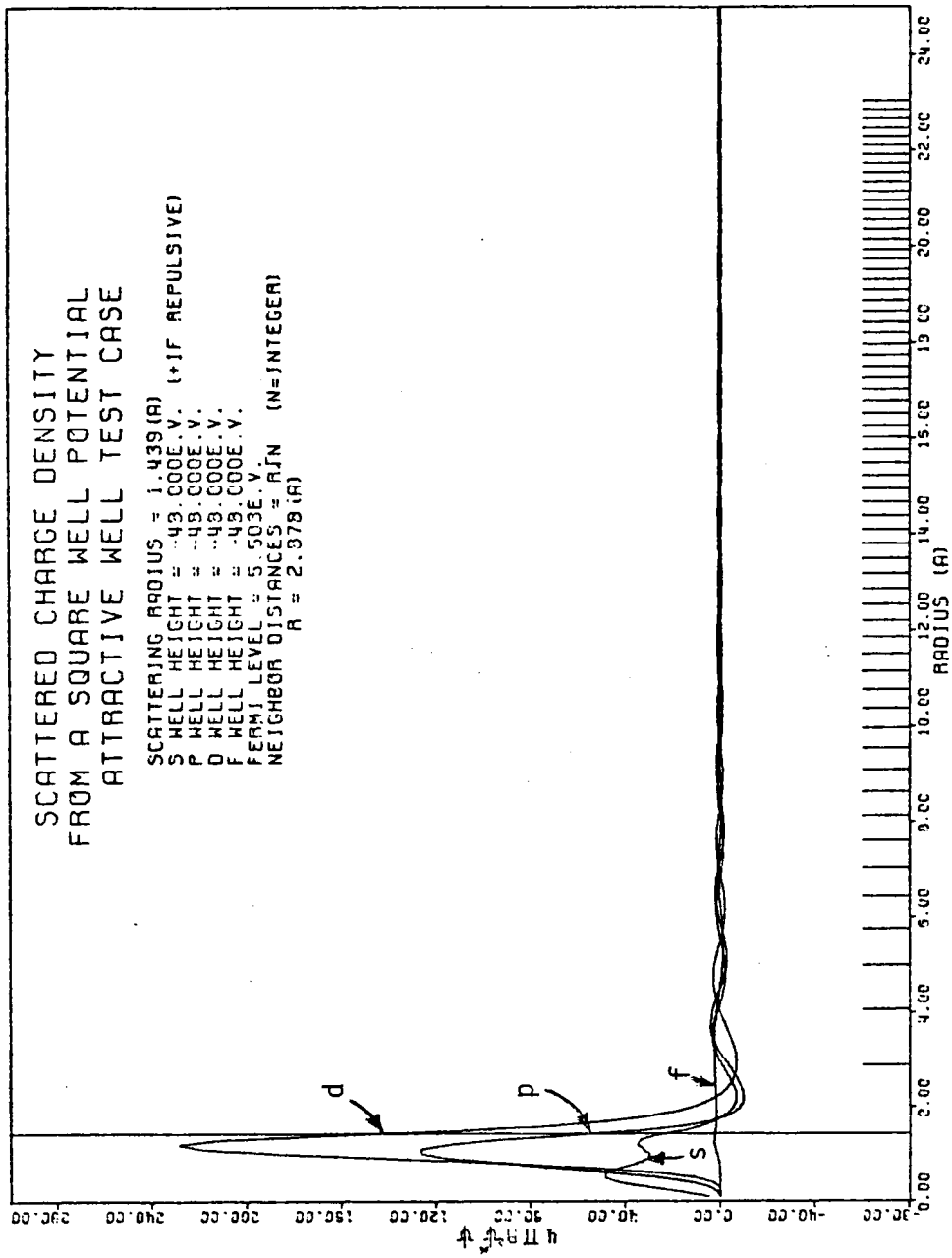


Figure 14. Scattered Charge Density for a -48 e.V. Height Well.

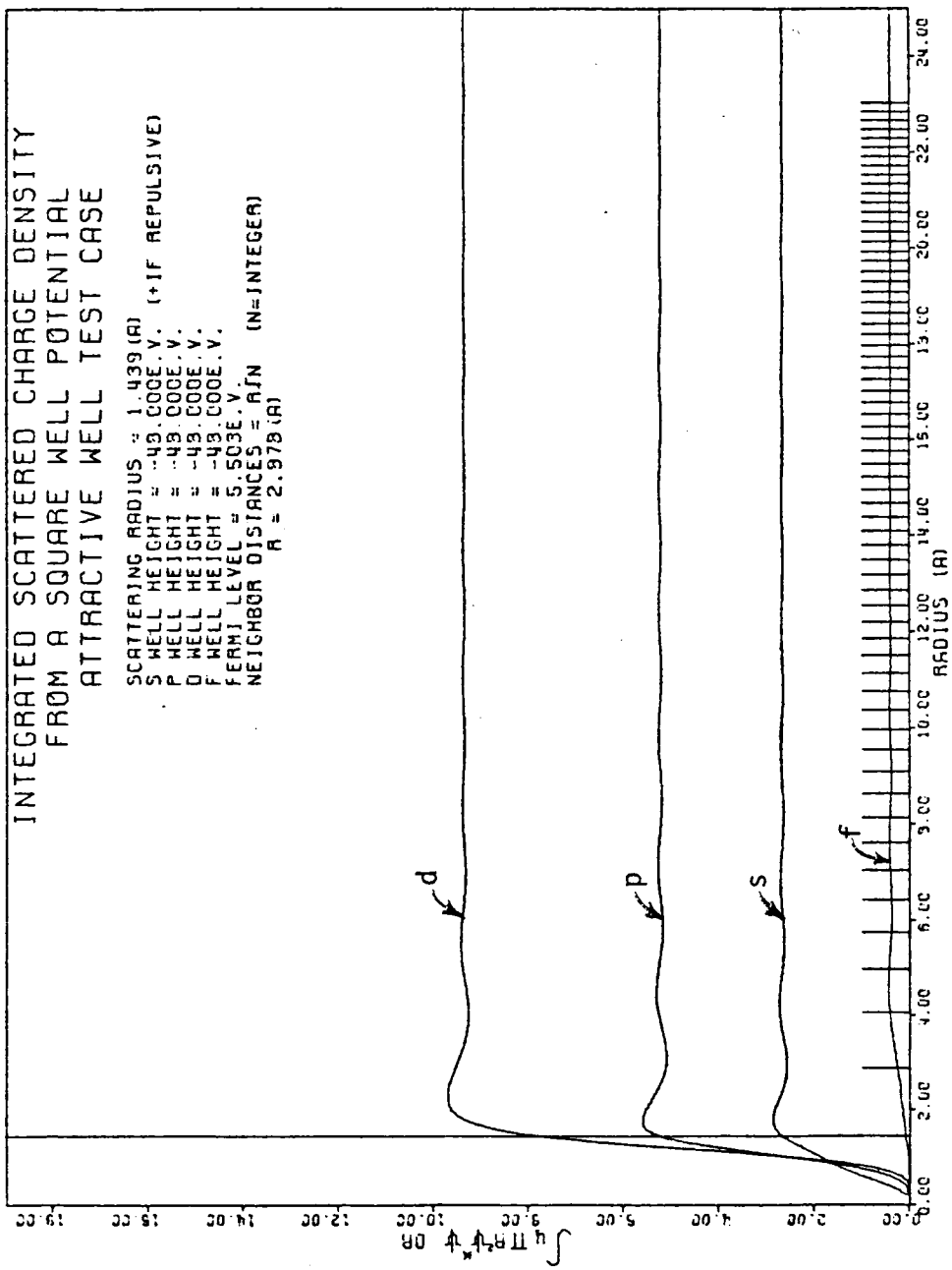


Figure 15. Integrated Scattered Charge Density for a -48 e.V. Height Well.

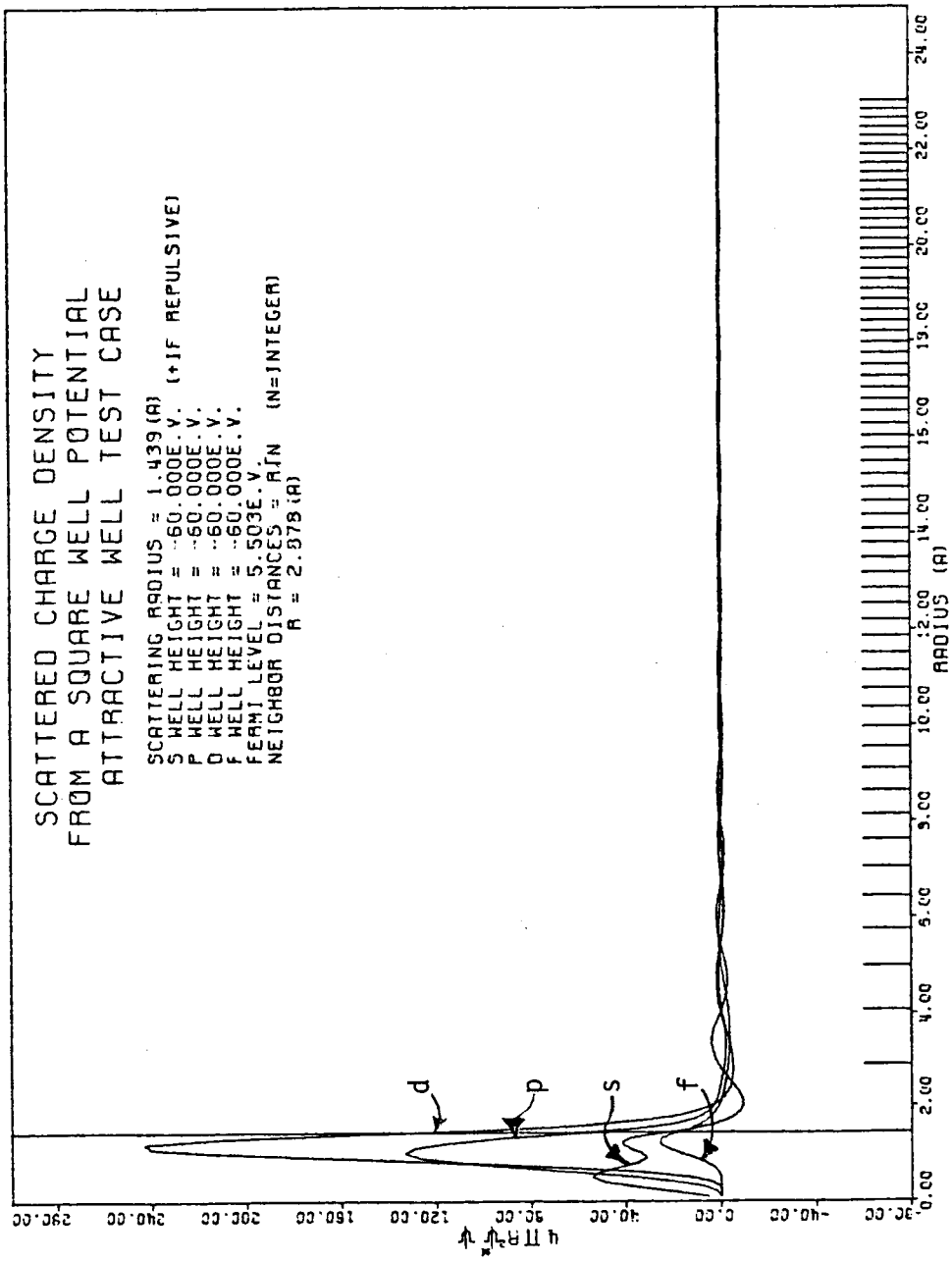


Figure 16. Scattered Charge Density for a -60 e.V. Height Well.

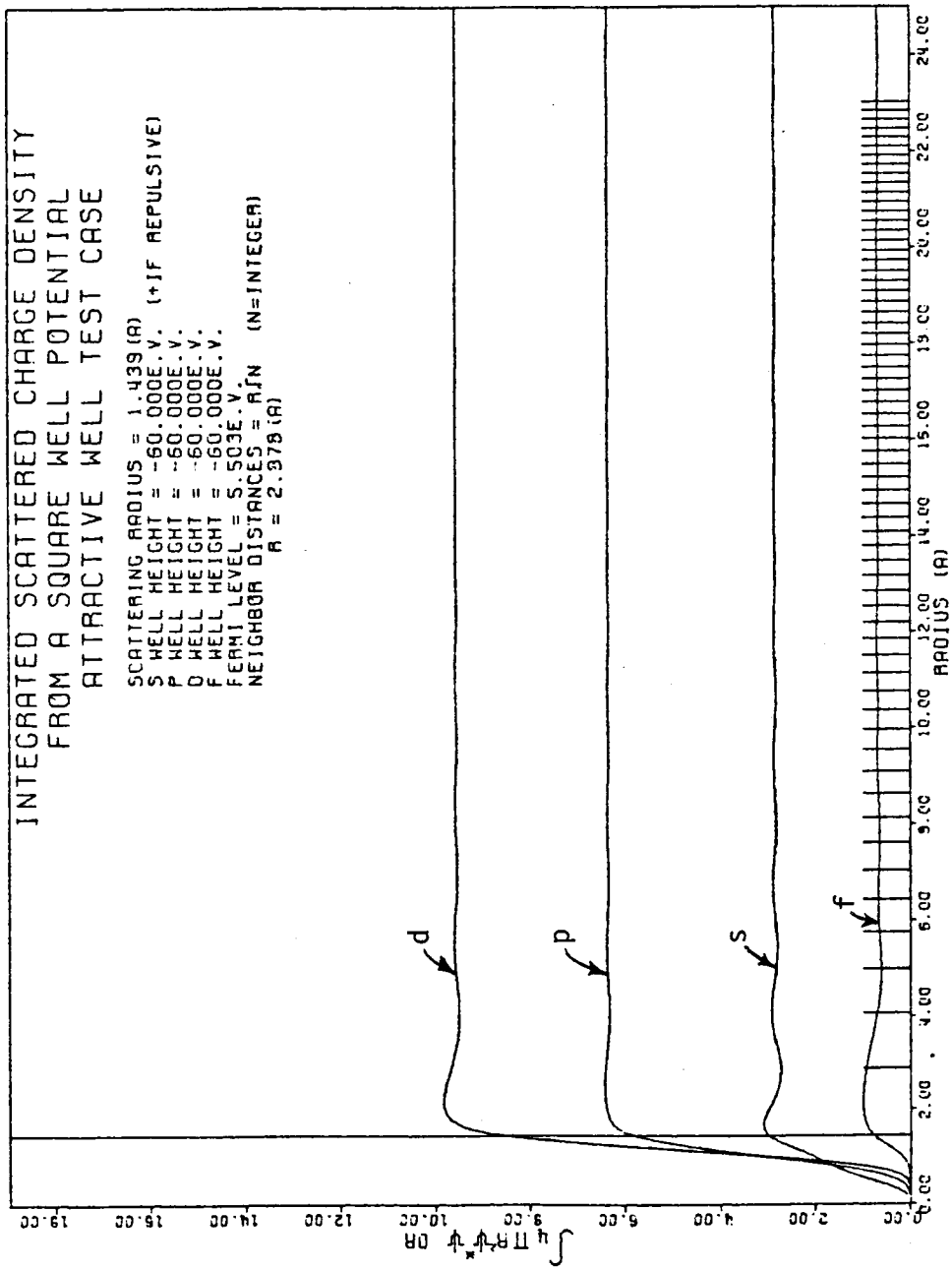


Figure 17. Integrated Scattered Charge Density for a -60 e.V. Height Well.

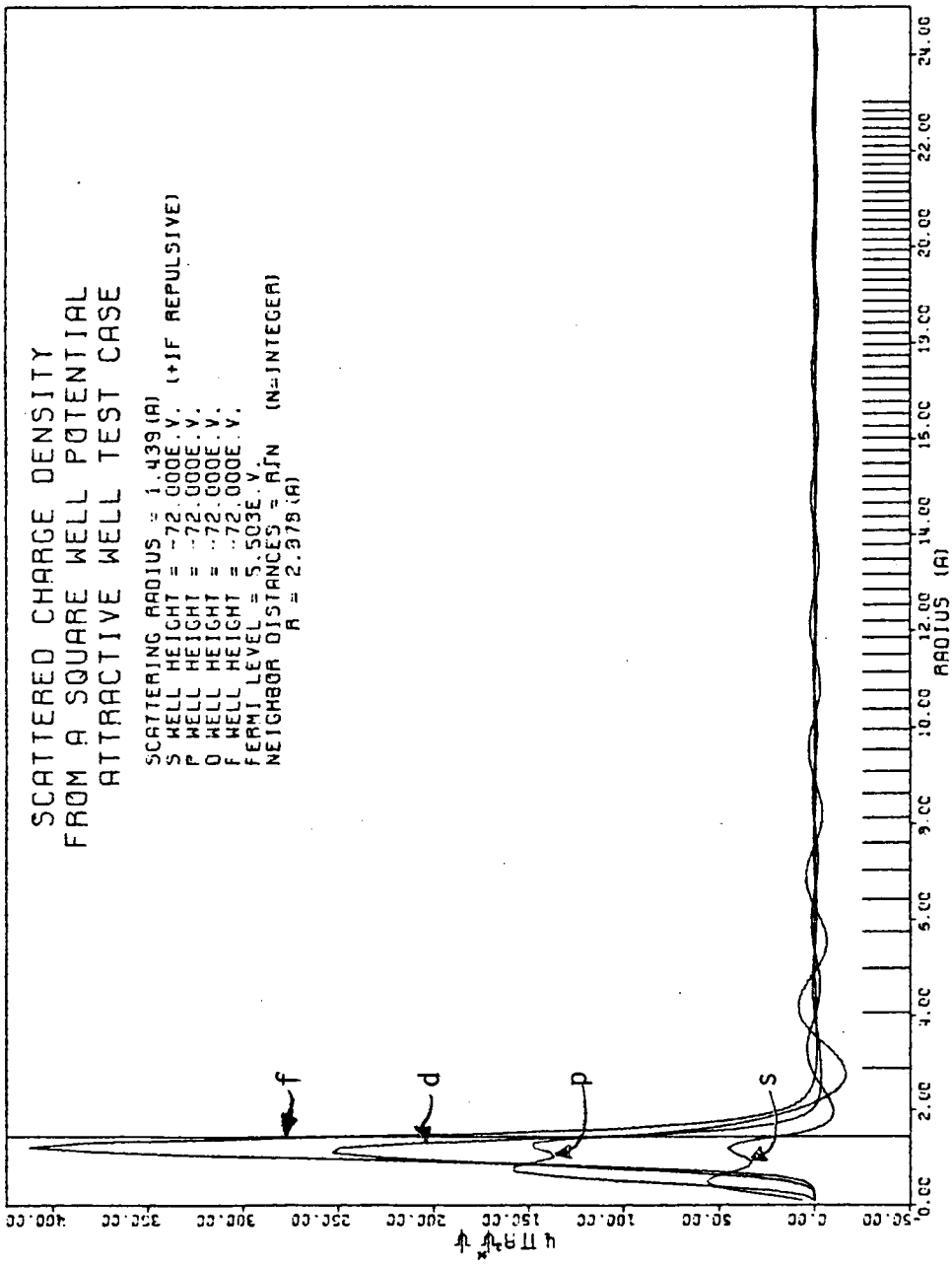


Figure 18. Scattered Charge Density for a -72 e.V. Height Well.

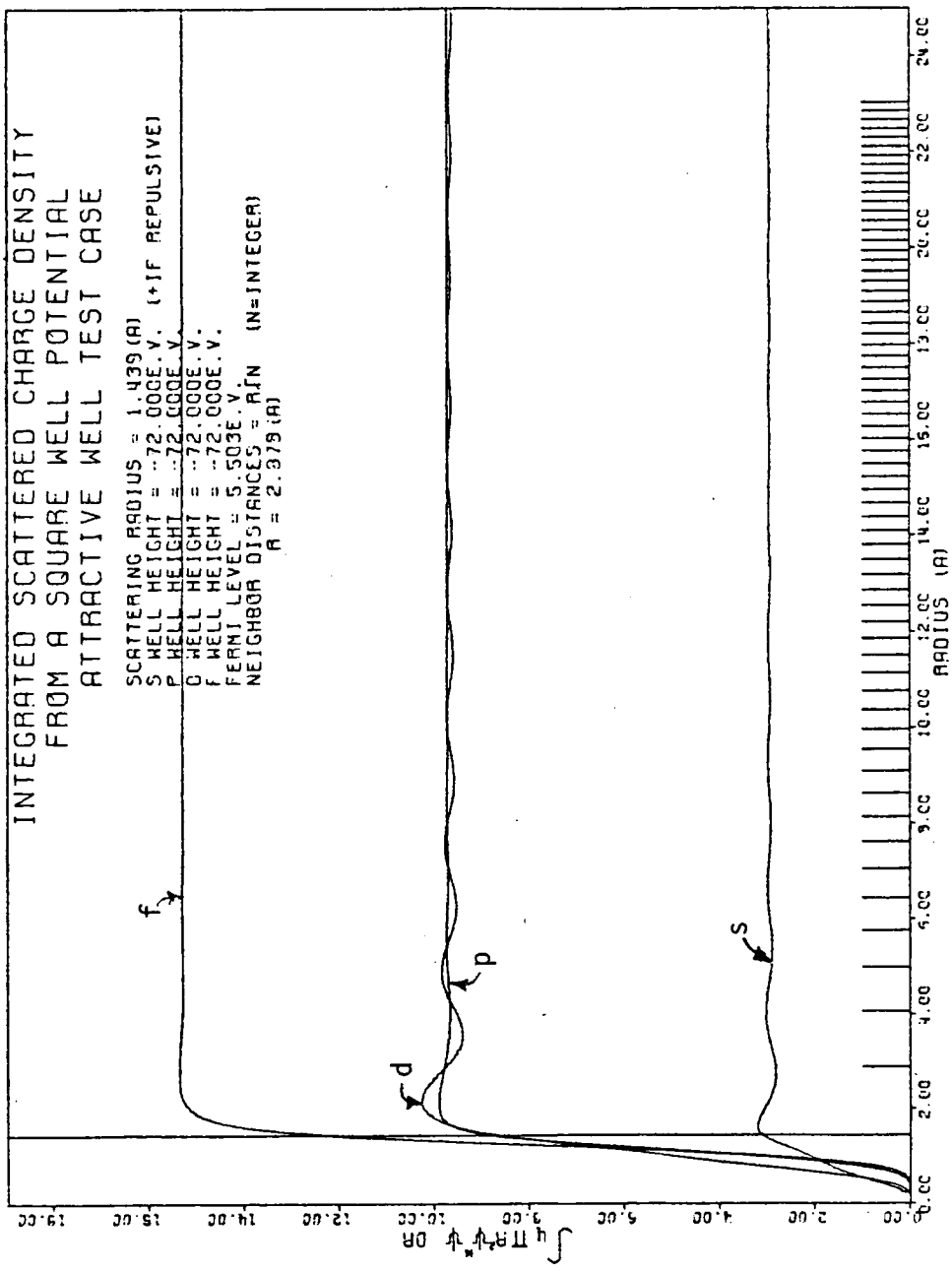


Figure 19. Integrated Scattered Charge Density for a -72 e.V. Height Well.

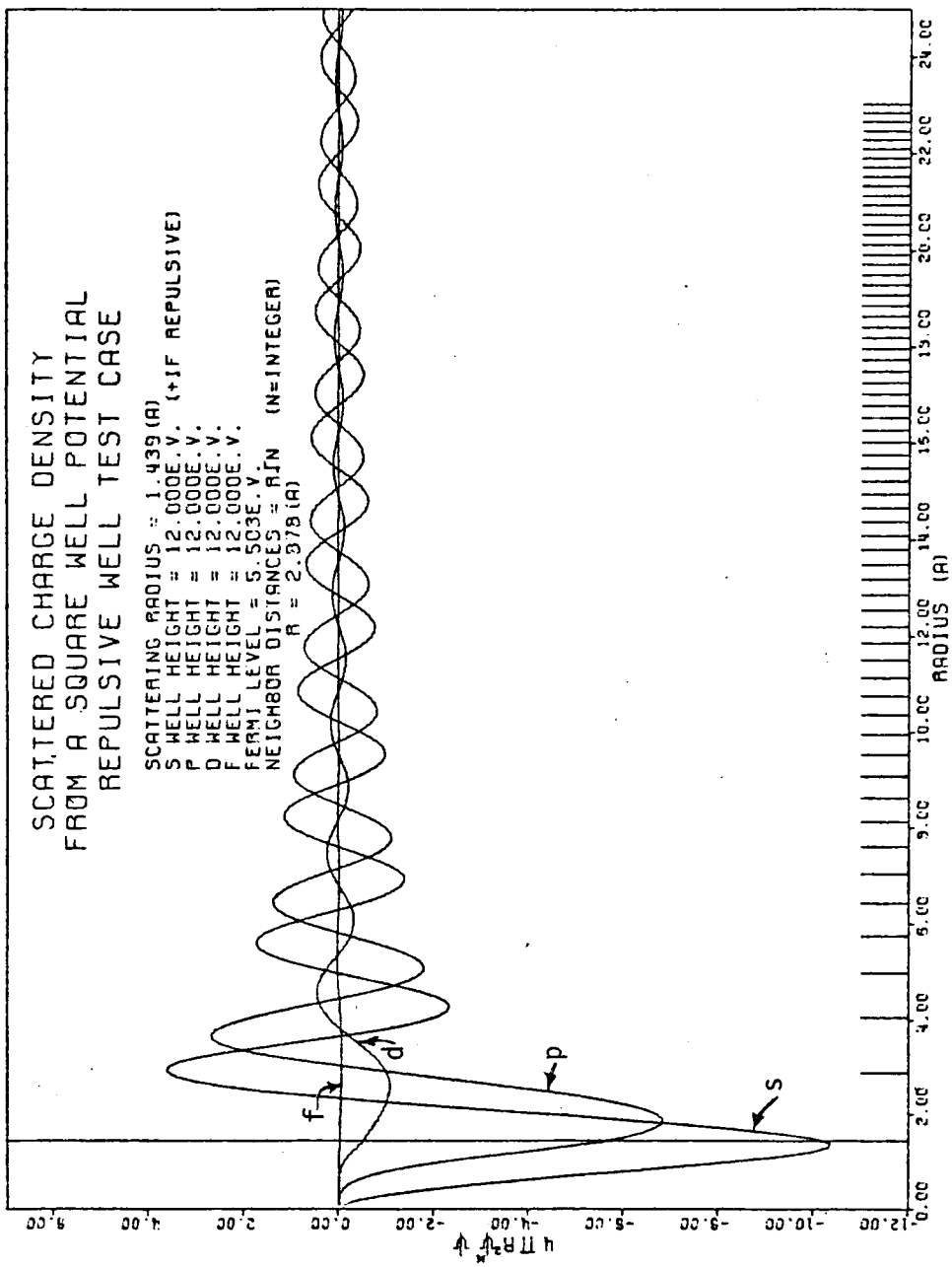


Figure 20. Scattered Charge Density for a +12 e.V. Height Well.

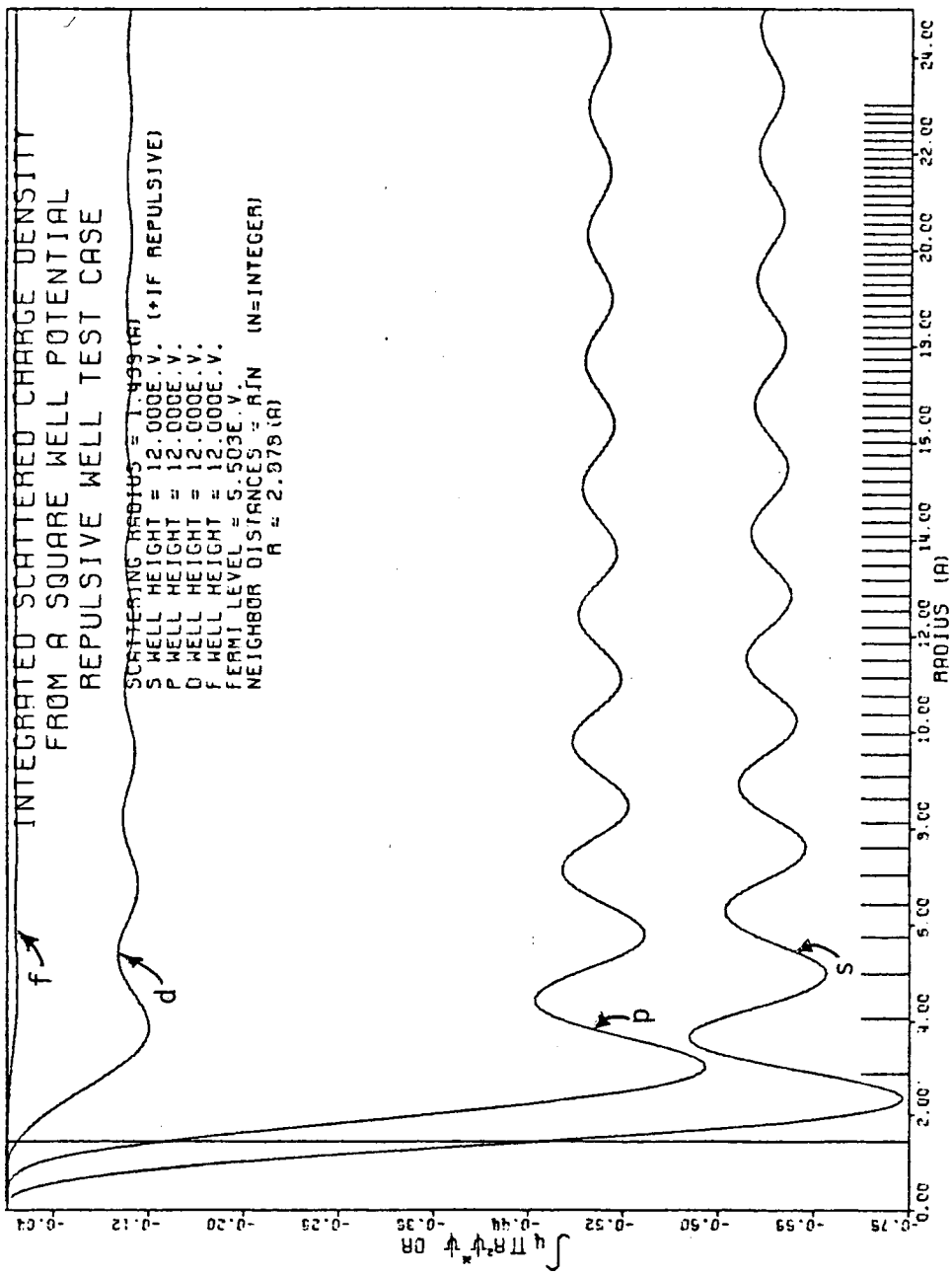


Figure 21. Integrated Scattered Charge Density for a +12 e.V. Height Well.

from the left hand side of the graph denotes the position of the scattering well boundary and is located 1.439A from the origin. The small vertical lines along the horizontal axis indicate the position in a radial sense of the neighboring atoms. For face centered cubic geometries there are 12 nearest neighbor atoms located 2.878A from the origin, there are six second near neighbor atoms located 4.0701A from the origin, and so forth. A given shell of atoms may be located by the expression $r = R\sqrt{N}$ where R = 2.878A and N is the shell number from the origin, i.e., N = 1, 2, 3, ... . On each graph there are 64 shell locations depicted.

Figure 10, p. 34, shows the fractional SCDD for a -12.0 e.V. well height. The charge density change inside the potential is dominantly due to the s and p SCDD while the d SCDD contributes little and the f SCDD is essentially zero for all values of r. At the near neighbor sites, the s, p, and d SCDD are once again dominant and the f SCDD is still essentially zero. It may also be noted that most of the charge density is within the well or at the first few near neighbor shells. Examining Figure 11, p. 35, it may be seen that the majority of the integrated SCDD associated with the scattering center is of p character accounting for approximately 2.45 electrons. The s integrated SCDD amounts to about 0.90 electrons, the d integrated SCDD amounts to 0.20 electrons, and the f integrated SCDD is negligible by comparison. (It may be noted in passing the agreement between our integrated charge and the value given by the Friedel sum rule (Equation I-18) is quite good for all of these angular momentum cases.)

A -28.0 e.V. height well for the fractional SCDD is shown in Figure 12, p. 36. As before the s and p SCDD make significant contributions

both inside and outside the well boundary but now the d SCDD is also seen to play a much more prominent role since the s and p electrons are more tightly attracted by the well. The integrated SCDD for the same well are shown in Figure 13, p. 37. As a check on the internal consistency of the programs, it should be noted that the final integrated s SCDD accounts for 1.35 electrons while the integrated p SCDD accounts for 4.57 electrons and the integrated d SCDD accounts for 5.09 electrons compared to Friedel sum rule values of 1.35, 4.56 and 5.08 electrons, respectively. As is the case until the well heights become very negative, the f SCDD is almost negligible yielding an integrated SCDD value of only 0.0473 electrons which may also be compared to Friedel sum rule value of 0.0473 electrons. So it is seen that the integrated SCDD for all four angular momentum states agree quite well with the original values given by the Friedel sum rule.

Trends that may be seen by examining Figures 10 through 21, pp. 34-45, are:

a. The first maximum of a SCDD grows larger as the well height becomes sufficiently deep to bind that angular momentum state SCDD.

b. As a well height becomes sufficiently negative to bind a particular angular momentum state SCDD, that SCDD becomes a much more prominent SCDD.

c. For well heights slightly more attractive than the binding energy, the SCDD that has just been bound may be quite small outside the well in comparison to the other distributions.

d. The total fractional scattered charge perturbation is seen to be concentrated predominantly within the wells and at the first few near neighbor shells with relatively little charge at more distant sites.

Figure 14, p. 38, has a well height of -48.0 e.V. and exhibits two peaks in the s SCDD inside the well boundary which arise from the binding of a second s angular momentum state. Figures 2 and 3, p. 9 and p. 13, respectively, have previously indicated that for wells of $E_{\ell m \sigma}$ = -40.8576 or less two s states are bound as in this case. Here the d SCDD is seen to play a dominant role relative to the other three SCDD. Figure 15, p. 39, shows that the f SCDD no longer makes a totally insignificant contribution to the total integrated charge. The first f bound state occurs at a well height of $E_{\ell m \sigma}$ = -61.1169 e.V. as shown by Figures 2 and 3, p. 9 and p. 13, respectively. Hence, Figures 16 and 17, pp. 40-41, for well heights of -60.0 e.V. show that the contribution of the f SCDD is just beginning to grow in amplitude relative to the s, p, and d contributions. Also in Figure 16, p. 40, it may be seen that within the well the d SCDD is still dominant since it has bound more electrons than the other states have. It is seen in Figure 17, p. 41, that the d SCDD still accounts for the major fraction of the total integrated charge density, as is expected, but that the f integrated SCDD is 7% of the contribution due to the d SCDD. The -72.0 e.V. case in Figure 18, p. 42, shows that after f electron binding has occurred, the f SCDD is the dominant term inside the well as well as to a lesser extent outside the well. It may also be seen, as predicted from Figure 2,

p. 9, and Figure 3, p. 13, that for this negative well height a second p electron state has been bound. The superposition of the two bound charge densities produces the double peaked charge distribution shown within the well boundary. Outside, the amplitude of the f charge density oscillations are of generally the same order of magnitude as the amplitude of the d charge density oscillations. The effect of the f electron is clearly demonstrated in Figure 19, p. 43, where 15.3 f electrons are seen to be associated with the -72.0 e.V. well height.

Repulsive wells show a behavior similar to that displayed by the attractive wells except that there are no bound states. Typical repulsive well results are shown in Figures 20 and 21, pp. 44-45, for a +12.0 e.V. high well. Since the charge is repulsed, the integrated and fractional SCDD show a negative behavior. As in the attractive case, only for relatively high barriers does the f SCDD contribute significantly to the total integrated or scattered charge density.

The preceding observations concerning the contribution of the f SCDD are also borne out in Figure 2, p. 9, which is a plot of the phase shift at the Fermi level versus well depth. The binding energies of the various angular momentum states are also indicated as has been previously noted several times. The s phase shift at the Fermi level is seen to vary the most in the range shown followed by the p, d, and f phase shifts in that order. Thus, there is not a significant change in the f SCDD until about -50.0 e.V. From approximately -50.0 e.V. down to the well height at which binding occurs there is a rather large change in the f phase shift corresponding to more f charge. The scale to the

right of this figure denotes the relative integrated charge density which corresponds to a given phase as may be obtained from Equation I-18. After the binding of the 14 f electrons (number of electrons bound is $2(2\ell+1)$) occurs, there is once again little change in the f phase shift with $k_F$ indicating that there is little change in the total f charge as was previously noted. The other three phase shifts vary more and sooner indicating once again that for small well heights the preponderance of charge is due to the first three angular momentum state wave functions and that only deep wells produce a significant amount of f charge.

For many dilute gold alloys, the required wells for a self-consistent solution of Equations I-28, I-29, and I-30 with S = 0 (see Equation I-20) have been found previously[3] (a discussion of self-consistent solutions is contained in the following section). The results of that analysis were that all the wells for s, p, and d angular momentum states fall within the range from approximately -40.0 e.V. to +28.0 e.V. with most wells only a few electron volts deep. These wells give integrated SCDD which are reasonably close to the valence difference between the impurity and gold atoms. The set of parameters found is given in Appendix II. Thus for the impurities studied (involving no f electrons in free atom pictures) it is felt that the f SCDD contributes a negligible amount to the total charge density.

## II. A SELF-CONSISTENT SOLUTION

In order to model the electronic charge density distribution for an alloy by the pseudo-potential technique used in this thesis, the well heights for the scatter of electrons need to be determined. It is reasonable

to assume that the lower order angular momentum states contribute the most fractional scattered charge density distribution as was argued in the previous section. The alloys studied have only s, p, and d electrons in their outer shells when in free atomic states and since large heights or extended potentials are associated with higher angular momentum scattering only s, p, and d scattering is considered. By determining the valence difference, N, between the host and impurity atoms, measuring the residual resistivity, $\frac{1}{\sigma}$, and measuring the differential Mössbauer isomer shift it is possible to solve for the well heights for the first angular momentum states which reproduce these experimentally determined quantities.

In terms of the first three phase shifts the Friedel sum rule is

$$N = \frac{2}{\pi}(\delta_0 + 3\delta_1 + 5\delta_2); \qquad \text{III-1}$$

likewise the residual resistivity, $\frac{1}{\sigma}$, may be expressed as

$$\frac{1}{\sigma} = m(1-m)\,\frac{4h}{ek_F}(\sin^2(\delta_0-\delta_1) + 2\sin^2(\delta_1-\delta_2) + 3\sin^2(\delta_2)); \qquad \text{III-2}$$

and the differential Mössbauer shift may be given by

$$\delta(\Delta E) = kn\rho_A(0)\left\{\left(\frac{\Omega_{Au}}{\Omega_B}\right)^{\gamma}\left(1 + m\,\frac{\langle\Delta\rho_{sc}\rangle_{total}}{\rho_A(0)}\right) - 1\right\} \qquad \text{III-3}$$

where

$$\frac{\langle \Delta\rho_{sc} \rangle}{\rho_A(0)}\text{total} = \sum_i \left( \frac{\langle \rho_{sc}(r_i) \rangle}{\rho_A(0)}\text{s} + \frac{\langle \rho_{sc}(r_i) \rangle}{\rho_A(0)}\text{p} + \frac{\langle \rho_{sc}(r_i) \rangle}{\rho_A(0)}\text{d} \right) \qquad \text{III-4}$$

with the summation extending over the neighboring shells of atoms. Measurement of the change in the lattice parameter and the differential Mössbauer isomer shift will thus give a relationship between the average s, p, and d fractional scattered charge densities. These densities may also be calculated as a function of phase shift from Equation I-17. Thus Equations III-1, III-2, and III-3 may be solved simultaneously by numerical techniques for the first three phase shifts $\delta_\ell(k_F)$. By solving the transcendental Equations I-7 or I-8, the corresponding well heights, $E_{\ell\sigma}$, may be determined. These well heights may be input to CHRGDN to produce plots of the fractional scattered charge density distributions as well as recalculating the residual resistivity and the differential Mössbauer isomer shift from the well heights as a check on the self-consistency of the solutions.

By calculating the fractional SCDD at the neighboring sites, the Mössbauer isomer shift for a particular configuration may be calculated by Equations III-3 and III-4. In this way the original absorption line may be reconstructed by considering the sum of all pure Lorentzian shaped lines for each possible configuration of impurities. The amplitude of each of the Lorentzian is assumed to be proportional to the associated probability of that configuration as given in Chapter II. The sum of the Lorentzian absorption lines produces an absorption line from which the effective line broadening may be determined. In this way the theory may be compared directly to experimental absorption spectra for

reproducing asymmetries and effective line broadening by means of this theoretical model.

## III. APPLICABILITY OF THE MODEL

The ultimate test of any model is its ability to reproduce experimental results. In the case of the pseudo-potential model presented herein, the most important piece of experimental data to be reproduced is the character of the Mössbauer absorption line. Other information produced by the model provides checks on its internal consistency. For a given alloy, a set of well heights with an associated set of phase shifts (Equation I-8) have been determined which are constrained to produce the measured residual resistivity, $\frac{1}{\sigma}$ (Equation I-25), the valence difference, N (Equation III-1) and the differential Mössbauer isomer shift, $\delta(\Delta E)$ (Equation III-3). Hence for an actual dilute alloy with measured values of the differential lattice parameter, residual resistivity, and differential Mössbauer isomer shift; Equation III-1, III-2, and III-3 may in principle be solved simultaneously for the first three phase shifts. Unfortunately, the equations are transcendental so that numerical techniques must be employed to find a set of phase shifts. Sometimes more than one set of phase shifts may satisfy Equations III-1, III-2, and III-3, thus implying that there may not be a unique charge density distribution which will result in the same values of observed residual resistivity, valence difference and differential Mössbauer isomer shift.

It is possible to give a graphical form of Equation III-3 by plotting the average scattered charge density versus phase shift or equivalently versus well height as is done in Figures 22 through 25. For the range of energies shown in Figure 22 the average s scattered charge density is seen to be positive for repulsive (positive height) wells which corresponds to the neighbors of the average seeing a net positive charge due to s character electrons. For attractive (negative height) wells there is a variation in sign of the average s scattered charge density. As may be seen from Figures 4 through 9, pp. 16-21, the average charge density at neighboring sites is only slightly affected by the presence of bound states. Similar characteristics may be noted for the p and d charge densities as shown in Figures 23 and 24. It is also seen that for the range of energies shown that the p average scattered charge density exhibits the most negative values whereas the d average scattered charge has the widest range. The f average scattered charge density (Figure 24) is seen to have the least variation in the range of energies shown until deep wells. This lends further credence to the previous arguments that (for deep well heights below $\pm$40 e.V.) the f angular momentum state wave functions contribute minimally to the total average scattered charge density which is obtained by adding all three (or four) average charge densities together.

Differential Mössbauer isomer shifts were reported by Kirthlink[10] in 1971 and residual resistivities were reported by Kwei[3] in 1976 for scandium, titanium, vanadium, chromium, manganese, iron, cobalt, nickel, copper, zinc, gallium, germanium, silver, cadmium, indium, and antimony in gold in a nominal mixture of one, two, and four percent atomic

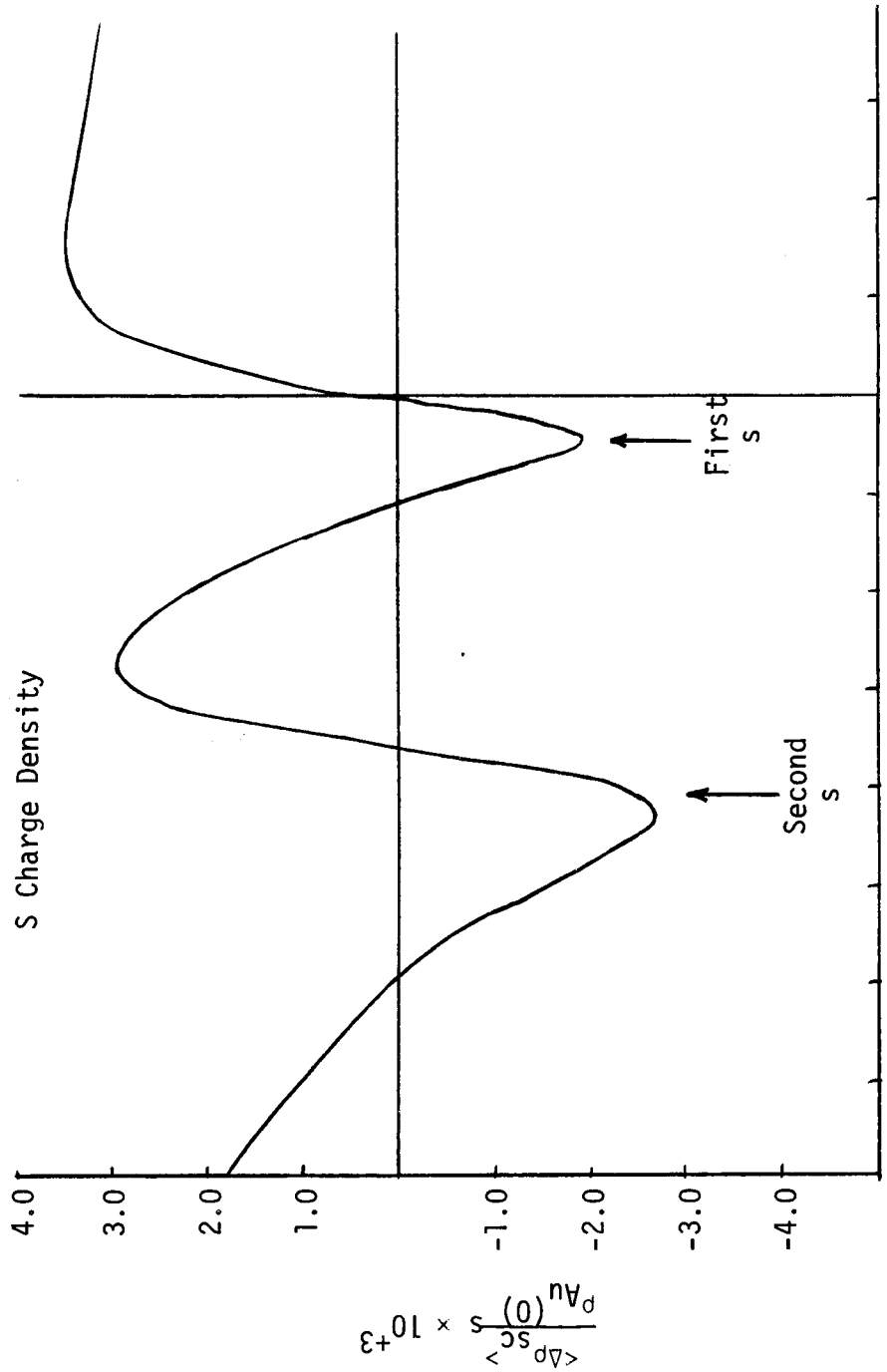


Figure 22. The Average Scattered Charge Density for s Angular Momentum,

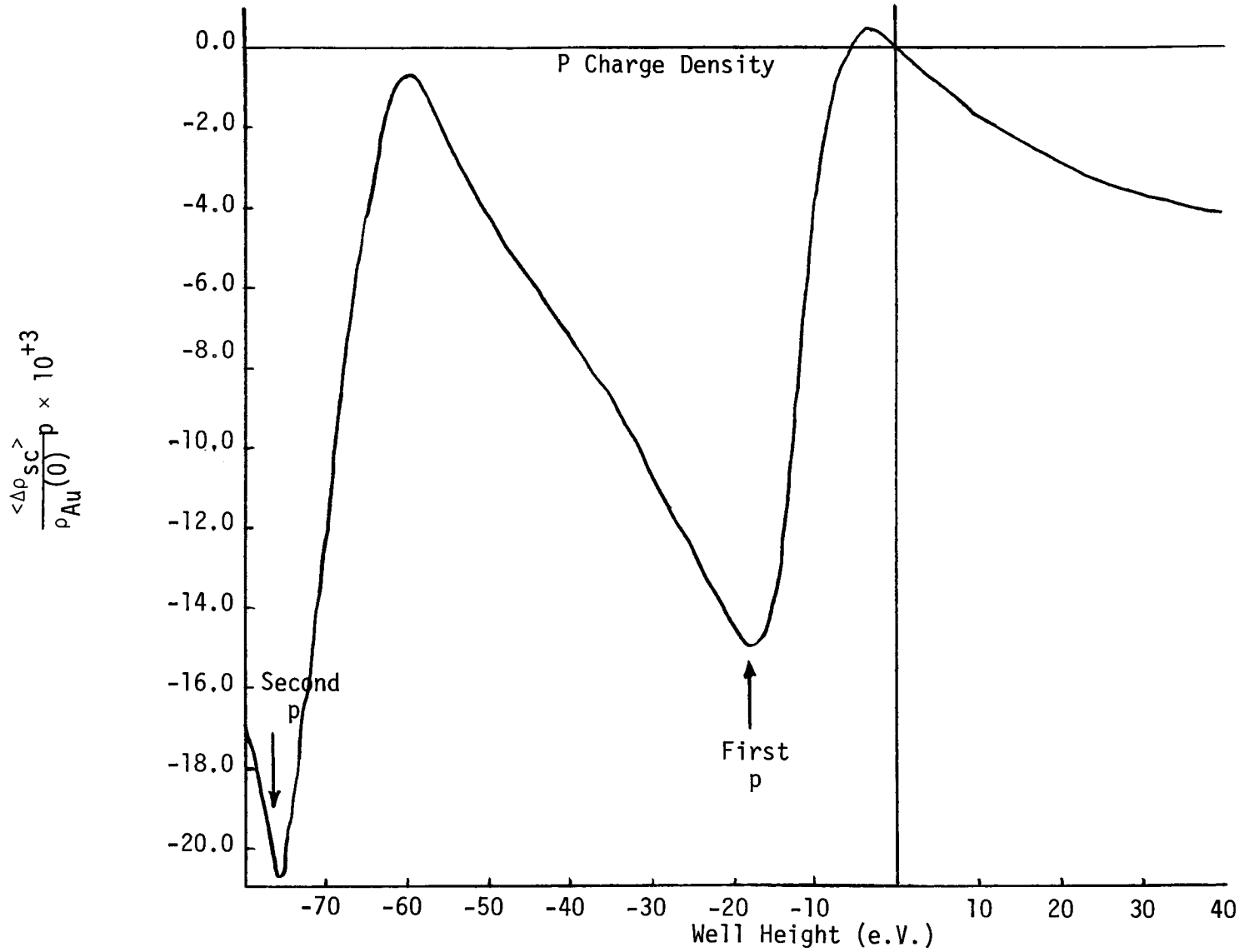


Figure 23. The Average Scattered Charge Density for p Angular Momentum.

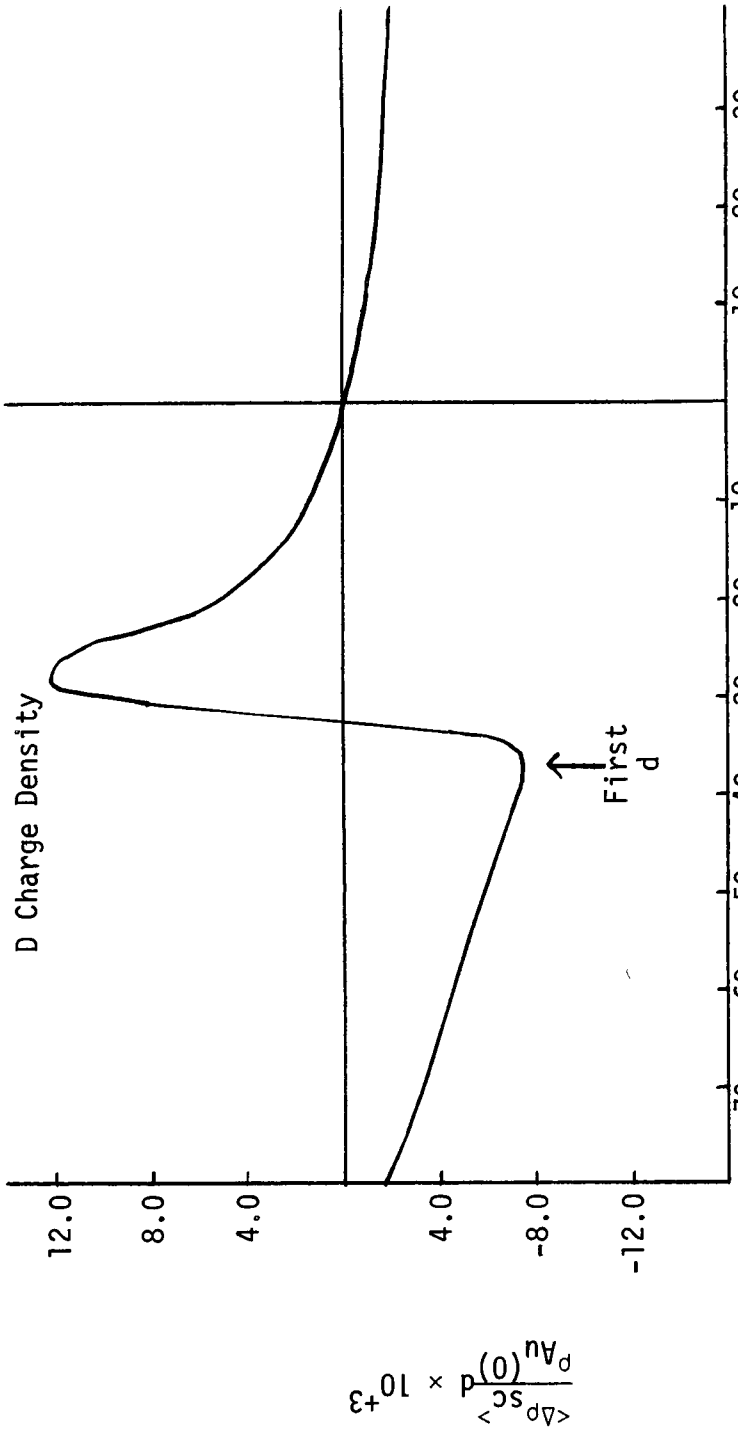


Figure 24. The Average Scattered Charge Density for d Angular Momentum.

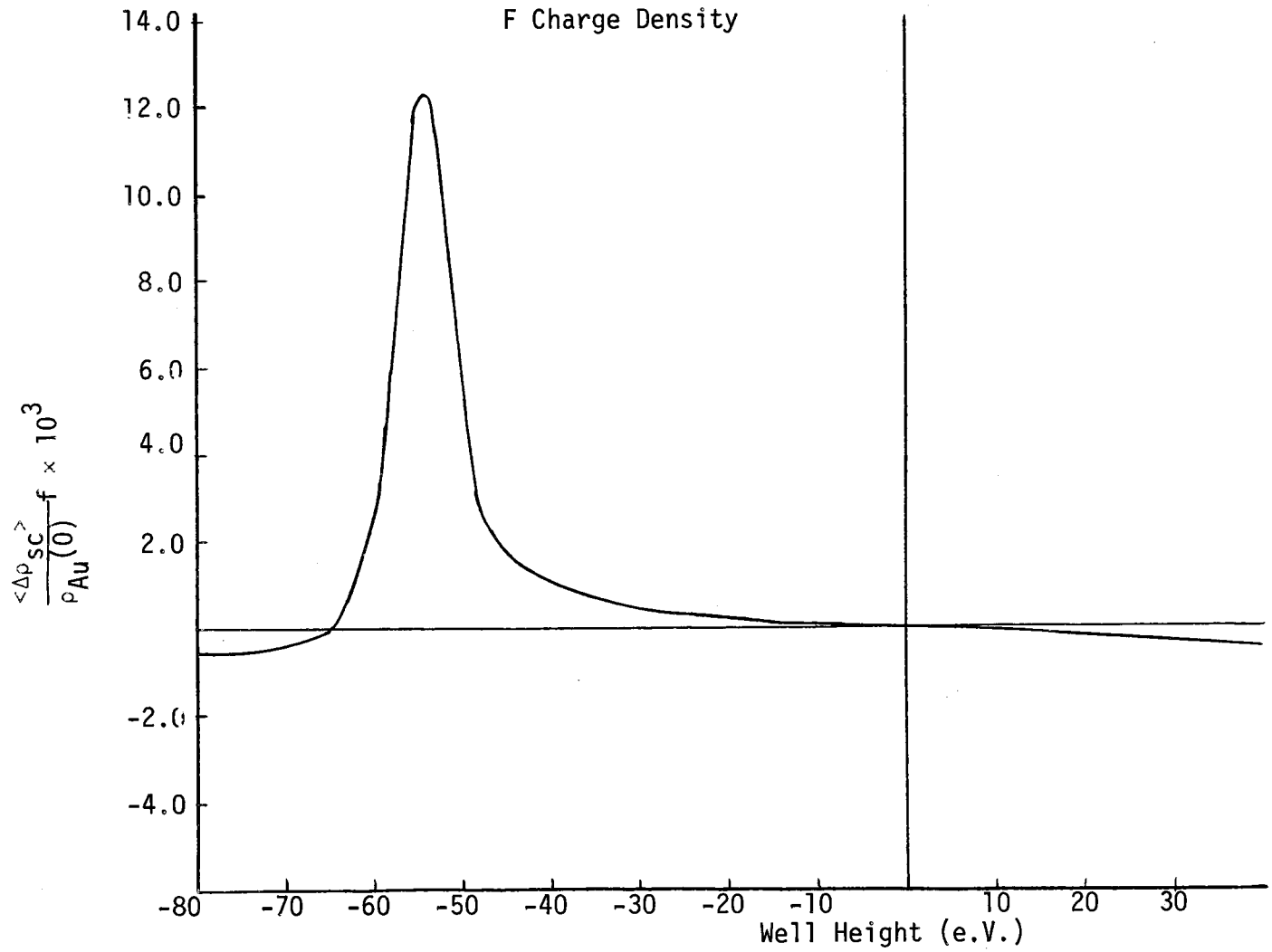


Figure 25. The Average Scattered Charge Density for f Angular Momentum.

impurity dissolved substitutionally into gold. Phase shifts (well heights) previously determined by Kwei[3] in 1976 were used in this work to check the agreement between theory and experiment. The results are found in Tables VII and VIII in Appendix II. The original calculations could not be found and hence values of phase shifts were taken from graphs given in that work. The agreement is reasonable in all cases except Sc, Co, Ni, and Ag.

It is also possible to reconstruct the original absorption spectra using the formalism of Chapter II. The quality of the model may thus be further tested by whether or not it is able to reproduce experimental results for a Vanadium alloy (Figure 26) which shows an asymmetry in the line shape. The solid line is a broadened symmetric Lorentzian which has been least squares fit to the data. A theoretical calculation by this model of the absorption line for the same alloy is shown by the asterisks in Figure 27. For ease of observation a symmetric broadened Lorentzian is also shown in this figure to indicate the degree of asymmetry. Manganese alloys showed no such experimental asymmetry as is seen in Figure 28. The theoretical plot generated by the model is shown in Figure 29 and the absorption line is seen to be symmetric. The fitting routine LORENT described in Chapter II is designed to fit a symmetric line to the spectra. Preliminary results yield a model line broadening of $\sim$0.2 mm/sec for both the V and Mn spectra by comparison to experimentally fit spectra values of $\sim$0.5 and $\sim$0.6 mm/sec, respectively. The model generated intensity is arbitrary and thus contains no experimentally comparable information. The total average scattered charge density may once again be determined by dividing the mean (isomer shift

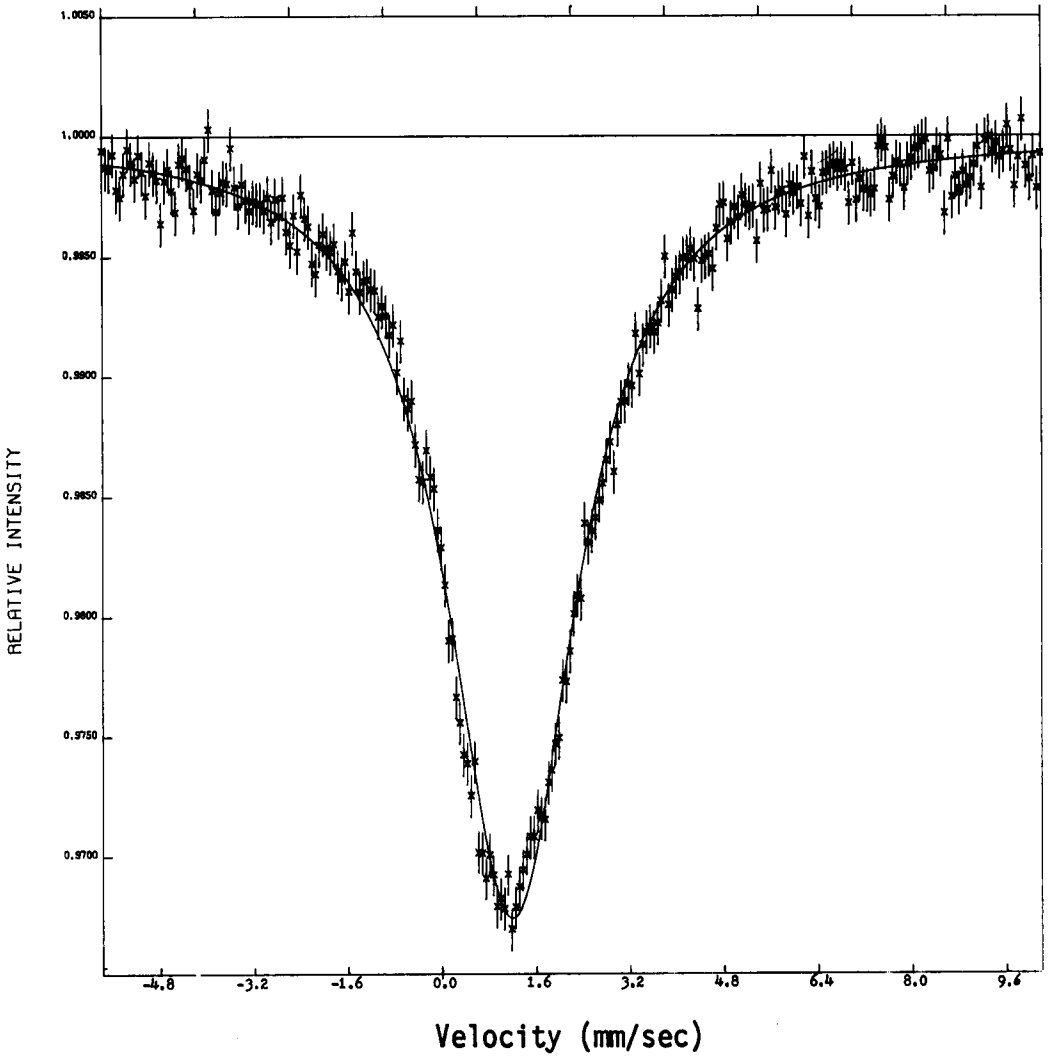


Figure 26. Experimental Spectrum for 1% Vanadium in Gold, Shifted by 1.2 mm/sec Due to Isomer Shift.

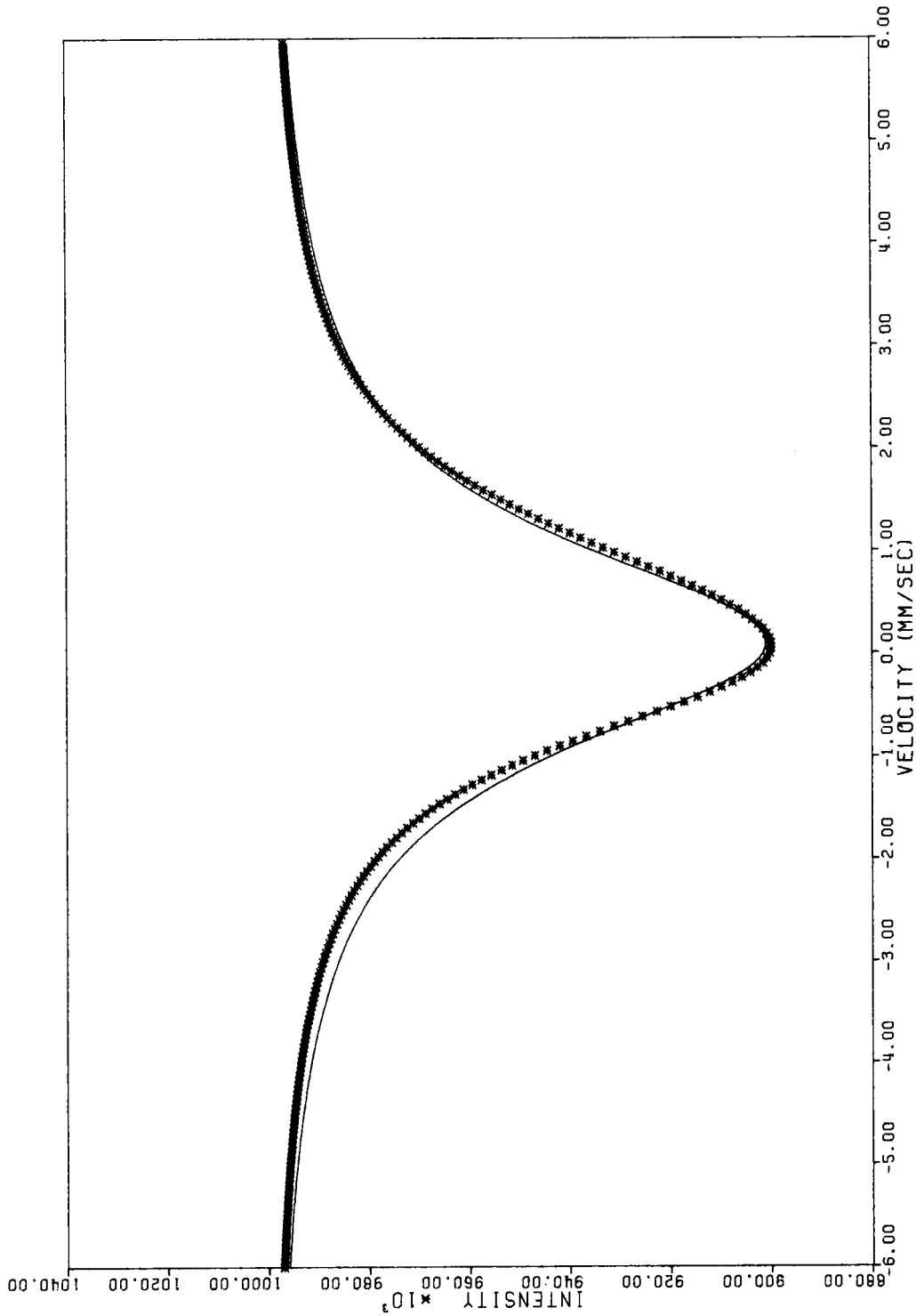


Figure 27. Generated Spectrum (asterisks) and Fit for 1% Vanadium in Gold.

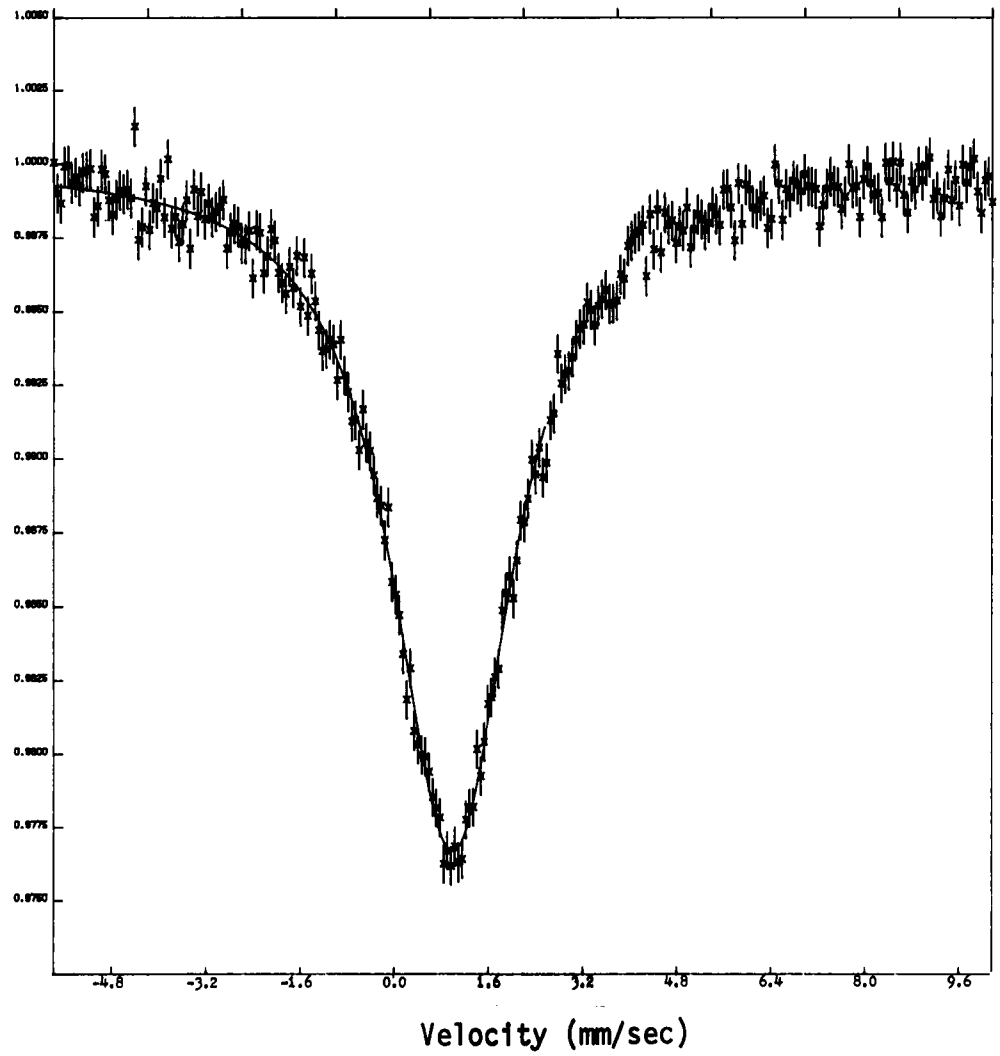


Figure 28. Experimental Spectrum for 1% Manganese in Gold, Shifted by 1.2 mm/sec Due to Isomer Shift.

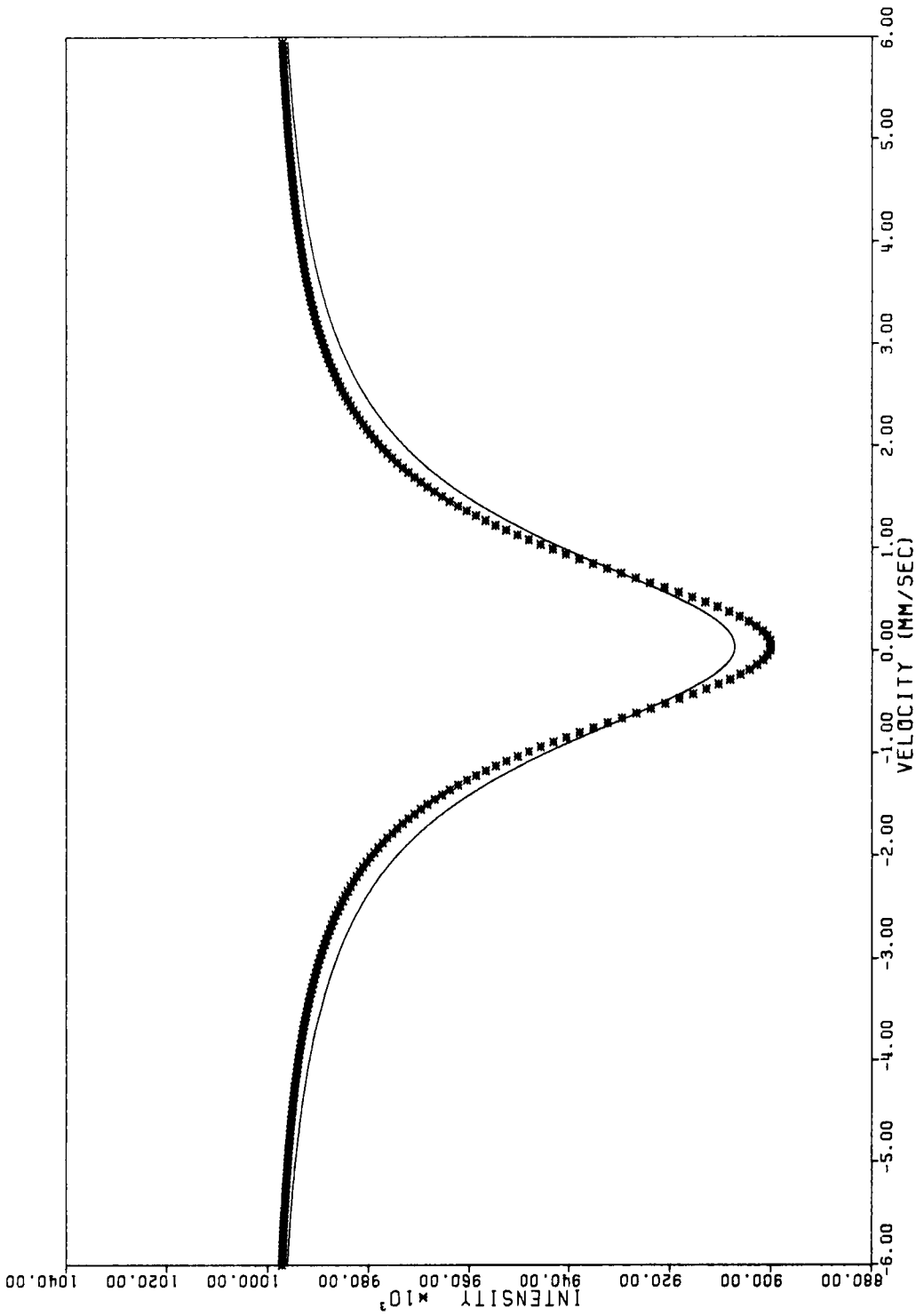


Figure 29. Generated Spectrum (asterisks) and Fit for 1% Manganese in Gold.

in mm/sec) of the model generated line by 8 mm/sec. The V fit gives a value of the total average scattered charge density as 0.0072 compared to the calculated value of 0.00679 using Equation III-3. The Mn fit gives a value of the total average scattered charge density as 0.00495 compared to 0.00465 for the calculated value of Equation III-3. An approximation to Equation II-1 was used to generate the model absorption lines by only using three, four, five and six sums. The discrepancies seen above may be due to these approximations, although the proper asymmetry characteristics of the Mössbauer absorption line is seen. The results for V give average scattered charge densities of 0.00572, 0.00826, and 0.0077 for three, four, five, and six shells, respectively. The expanded computer codes should be of interest in predicting several different experimentally measurable quantities such as the Knight Shift and the nuclear specific heat for dilute gold as well as dilute copper alloys.

# LIST OF REFERENCES

## LIST OF REFERENCES


1. Louis D. Roberts, Richard L. Becker, F. E. Obenshain, and J. O. Thomson, Phys. Rev. 137, A895 (1965).

2. P. G. Huray, C. M. Tung, F. E. Obenshain, and J. O. Thomson, Journal De Physique, 37, C6-371 (1976).

3. Cheng-May Kwei, Dissertation, University of Tennessee (1976).

4. Phillip M. Morse and Hermann Feshbach, Methods of Theoretical Physics, 2 (McGraw-Hill, New York, 1953).

5. J. Friedel, Nuovo Cimento, 7, 287 (1958); Can. J. Phys. 34, 1190 (1956).

6. F. J. Blatt, Phys. Rev. 108, 285 and 1204 (1957).

7. J. M. Ziman, Principles of the Theory of Solids, (University Press, Cambridge, 1972).

8. S. D. Conte and Carl De Boor, Elementary Numerical Analysis, 2nd ed. (McGraw-Hill, St. Louis, 1972).

9. Philip R. Bevington, Data Reduction and Error Analysis for the Physical Sciences, (McGraw-Hill, St. Louis, 1969).

10. Townsend Justin Kirthlink, Jr., Thesis, University of Tennessee (1971).

# APPENDIXES

# APPENDIX I

TABLE I

FIRST s ELECTRON BOUND STATE ENERGIES

| Well Depth (E. V.) | $k'_{b0}a$ | $E_{b0}$ (E. V.) |
|---|---|---|
| 5.0 | 1.644078894 | 0.026803638 |
| 6.0 | 1.770098340 | 0.235188846 |
| 8.0 | 1.942676976 | 1.056291430 |
| 10.0 | 2.058991331 | 2.199915004 |
| 12.0 | 2.144697015 | 3.537041211 |
| 14.0 | 2.211462405 | 5.001928902 |
| 16.0 | 2.265499330 | 6.556821995 |
| 18.0 | 2.310473664 | 8.178171547 |
| 20.0 | 2.348712805 | 9.850371875 |
| 22.0 | 2.381777857 | 11.56258852 |
| 24.0 | 2.410761772 | 13.30701665 |
| 26.0 | 2.436456537 | 15.07786259 |
| 28.0 | 2.459452511 | 16.87071711 |
| 30.0 | 2.480200291 | 18.68215330 |
| 32.0 | 2.499050779 | 20.50945942 |
| 34.0 | 2.516282010 | 22.35045605 |
| 36.0 | 2.532117612 | 24.20336758 |
| 38.0 | 2.546739849 | 26.06673002 |
| 40.0 | 2.560299011 | 27.93932330 |
| 42.0 | 2.572920324 | 29.82012100 |
| 44.0 | 2.584709105 | 31.70825210 |
| 46.0 | 2.595754677 | 33.60297178 |
| 48.0 | 2.606133379 | 35.50363860 |
| 50.0 | 2.615910909 | 37.40969657 |
| 52.0 | 2.625144165 | 39.32066093 |
| 54.0 | 2.633882718 | 41.23610673 |
| 56.0 | 2.642169982 | 43.15565959 |
| 58.0 | 2.650044176 | 45.07898811 |
| 60.0 | 2.657539092 | 47.00579773 |
| 62.0 | 2.664684746 | 48.93582555 |
| 64.0 | 2.671507898 | 50.86883604 |
| 66.0 | 2.678032502 | 52.80461744 |
| 68.0 | 2.684280069 | 54.74297875 |
| 70.0 | 2.690269986 | 56.68374718 |
| 72.0 | 2.696019774 | 58.62676595 |
| 74.0 | 2.701545317 | 60.57189239 |
| 76.0 | 2.706861054 | 62.51899636 |
| 78.0 | 2.711980144 | 64.46795884 |
| 80.0 | 2.716914611 | 66.41867077 |

TABLE I (Continued)

| Well Depth (E. V.) | $k'_{b0}a$ | $E_{b0}$ (E.V.) |
|---|---|---|
| 82.0 | 2.721675463 | 68.37103190 |
| 84.0 | 2.726272807 | 70.32495001 |
| 86.0 | 2.730715935 | 72.28034003 |
| 88.0 | 2.735013411 | 74.23712329 |
| 90.0 | 2.739173145 | 76.19522700 |
| 92.0 | 2.743202450 | 78.15458368 |
| 94.0 | 2.747108105 | 80.11513060 |
| 96.0 | 2.750896401 | 82.07680938 |
| 98.0 | 2.754573186 | 84.03956568 |
| 100.0 | 2.758143906 | 86.00334874 |

Binding occurs when $E_0 < -4.5397$ e.V.

TABLE II

SECOND s ELECTRON BOUND STATE ENERGIES

| Well Depth (E. V.) | $k'_{b0}a$ | $E_{b0}$ (E. V.) |
|---|---|---|
| 41.0 | 4.720442320 | 0.002659055 |
| 42.0 | 4.769913846 | 0.138829376 |
| 44.0 | 4.846403151 | 0.785511646 |
| 46.0 | 4.906374325 | 1.709390471 |
| 48.0 | 4.956397426 | 2.801653787 |
| 50.0 | 4.999554708 | 4.011107702 |
| 52.0 | 5.037601082 | 5.308497869 |
| 54.0 | 5.071654400 | 6.675111220 |
| 56.0 | 5.102481273 | 8.098056097 |
| 58.0 | 5.130635660 | 9.567972516 |
| 60.0 | 5.156533782 | 11.07779383 |
| 62.0 | 5.180497949 | 12.62202092 |
| 64.0 | 5.202783827 | 14.19627090 |
| 66.0 | 5.223598233 | 15.79698138 |
| 68.0 | 5.243111215 | 17.42120964 |
| 70.0 | 5.261464530 | 19.06649153 |
| 72.0 | 5.278777749 | 20.73073945 |
| 74.0 | 5.295152765 | 22.41216680 |
| 76.0 | 5.310677184 | 24.10923120 |
| 78.0 | 5.325426926 | 25.82059067 |
| 80.0 | 5.339468248 | 27.54506957 |
| 82.0 | 5.352859337 | 29.28163155 |
| 84.0 | 5.365651585 | 31.02935805 |
| 86.0 | 5.377890615 | 32.78743079 |
| 88.0 | 5.389617124 | 34.55511741 |
| 90.0 | 5.400867566 | 36.33175974 |
| 92.0 | 5.411674725 | 38.11676414 |
| 94.0 | 5.422068197 | 39.90959288 |
| 96.0 | 5.432074782 | 41.70975779 |
| 98.0 | 5.441718833 | 43.51681396 |
| 100.0 | 5.451022541 | 45.33035486 |

Binding occurs when $E_0 < -40.8576$ E. V.

TABLE III

FIRST p ELECTRON BOUND STATE ENERGIES

| Well Depth (E. V.) | $k'_{b1}a$ | $E_{b1}$ (E. V.) |
|---|---|---|
| 19.0 | 3.183255288 | 0.356251433 |
| 20.0 | 3.225285688 | 0.860672318 |
| 22.0 | 3.295387063 | 2.019646695 |
| 24.0 | 3.353063610 | 3.314125597 |
| 26.0 | 3.402076540 | 4.704960056 |
| 28.0 | 3.444593920 | 6.169365398 |
| 30.0 | 3.482033806 | 7.692224480 |
| 32.0 | 3.515389556 | 9.262787764 |
| 34.0 | 3.545389079 | 10.87306370 |
| 36.0 | 3.572583485 | 12.51691923 |
| 38.0 | 3.597400698 | 14.18953220 |
| 40.0 | 3.620179805 | 15.88703692 |
| 42.0 | 3.641194064 | 17.60628469 |
| 44.0 | 3.660666849 | 19.34467614 |
| 46.0 | 3.678783019 | 21.10004024 |
| 48.0 | 3.695697206 | 22.87054543 |
| 50.0 | 3.711539996 | 24.65463274 |
| 52.0 | 3.726422603 | 26.45096449 |
| 54.0 | 3.740440468 | 28.25838487 |
| 56.0 | 3.753676054 | 30.07588862 |
| 58.0 | 3.766201065 | 31.90259637 |
| 60.0 | 3.778078203 | 33.73773463 |
| 62.0 | 3.789362584 | 35.58061984 |
| 64.0 | 3.800102896 | 37.43064500 |
| 66.0 | 3.810342337 | 39.28726896 |
| 68.0 | 3.820119394 | 41.15000731 |
| 70.0 | 3.829468490 | 43.01842484 |
| 72.0 | 3.838420525 | 44.89212934 |
| 74.0 | 3.847003331 | 46.77076603 |
| 76.0 | 3.855242051 | 48.65401322 |
| 78.0 | 3.863159471 | 50.54157822 |
| 80.0 | 3.870776302 | 52.43319428 |
| 82.0 | 3.878111407 | 54.32861729 |
| 84.0 | 3.885182024 | 56.22762375 |
| 86.0 | 3.892003930 | 58.13000831 |
| 88.0 | 3.898591606 | 60.03558196 |
| 90.0 | 3.004958367 | 61.94417041 |
| 92.0 | 3.911116484 | 63.85561260 |
| 94.0 | 3.917077285 | 65.76975941 |
| 96.0 | 3.922851247 | 67.68647256 |
| 98.0 | 3.928448079 | 69.60562365 |
| 100.0 | 3.933876792 | 71.52709321 |

Binding occurs when $E_1 < -18.1589$ e.V.

TABLE IV

SECOND p ELECTRON BOUND STATE ENERGIES

| Well Depth (E. V.) | $k'_{b1}a$ | $E_{b1}$ (E.V.) |
|---|---|---|
| 73.0 | 6.292783012 | 0.142240483 |
| 74.0 | 6.316014270 | 0.603305050 |
| 76.0 | 6.355655476 | 1.679094326 |
| 78.0 | 6.389761555 | 2.879304078 |
| 80.0 | 6.420080116 | 4.164737524 |
| 82.0 | 6.447523760 | 5.515012250 |
| 84.0 | 6.472665847 | 6.917343589 |
| 86.0 | 6.495902329 | 8.362905913 |
| 88.0 | 6.517523421 | 9.845228113 |
| 90.0 | 6.537750848 | 11.35936160 |
| 92.0 | 6.556759322 | 12.90140237 |
| 94.0 | 6.574689848 | 14.46819492 |
| 96.0 | 6.591658424 | 16.05713883 |
| 98.0 | 6.607761994 | 17.66605735 |
| 100.0 | 6.623082652 | 19.29310329 |

Binding occurs when $E_1 < -72.6357$ e.V.

TABLE V

FIRST d ELECTRON BOUND STATE ENERGIES

| Well Depth (E. V.) | $k'_{b2}a$ | $E_{b2}$ (E. V.) |
|---|---|---|
| 38.0 | 4.513089598 | 0.525296092 |
| 40.0 | 4.554322662 | 1.837405657 |
| 42.0 | 4.590580981 | 3.227339272 |
| 44.0 | 4.623096167 | 4.676138853 |
| 46.0 | 4.652604859 | 6.172537376 |
| 48.0 | 4.679616372 | 7.708744315 |
| 50.0 | 4.704508390 | 9.278966319 |
| 52.0 | 4.727573210 | 10.87870105 |
| 54.0 | 4.749043790 | 12.50434280 |
| 56.0 | 4.769109862 | 14.15293988 |
| 58.0 | 4.787928586 | 15.82203452 |
| 60.0 | 4.805631928 | 17.50955227 |
| 62.0 | 4.822331959 | 19.21372237 |
| 64.0 | 4.838124772 | 20.93301910 |
| 66.0 | 4.853093447 | 22.66611698 |
| 68.0 | 4.867310335 | 24.41185634 |
| 70.0 | 4.880838852 | 26.16921620 |
| 72.0 | 4.893734901 | 27.93729267 |
| 74.0 | 4.906048020 | 29.71528150 |
| 76.0 | 4.917822315 | 31.50246375 |
| 78.0 | 4.929097222 | 33.29819419 |
| 80.0 | 4.939908144 | 35.10189146 |
| 82.0 | 4.950286978 | 36.91302981 |
| 84.0 | 4.960262562 | 38.73113246 |
| 86.0 | 4.969861048 | 40.55576552 |
| 88.0 | 4.979106224 | 42.38653316 |
| 90.0 | 4.988019784 | 44.22307315 |
| 92.0 | 4.996621568 | 46.06505343 |
| 94.0 | 5.004929762 | 47.91216865 |
| 96.0 | 5.012961073 | 49.76413752 |
| 98.0 | 5.020730885 | 51.62070039 |
| 100.0 | 5.028253393 | 53.48161704 |

Binding occurs when $E_2 < -37.1484$ e.V.

TABLE VI

FIRST f ELECTRON BOUND STATE ENERGIES

| Well Depth (E. V.) | $k'_{b3}a$ | $E_{b3}$ (E. V.) |
|---|---|---|
| 62.0 | 5.775113171 | 0.636333993 |
| 64.0 | 5.799877172 | 2.108944185 |
| 66.0 | 5.822781593 | 3.619148328 |
| 68.0 | 5.844129009 | 5.160909930 |
| 70.0 | 5.86413360l | 6.729974243 |
| 72.0 | 5.882959324 | 8.323088591 |
| 74.0 | 5.900737234 | 9.937652374 |
| 76.0 | 5.917575091 | 11.57152465 |
| 78.0 | 5.933563307 | 13.22290619 |
| 80.0 | 5.948778909 | 14.89026090 |
| 82.0 | 5.963288316 | 16.57226084 |
| 84.0 | 5.977149374 | 18.26774709 |
| 86.0 | 5.990412871 | 19.97569920 |
| 88.0 | 6.003123722 | 21.69521256 |
| 90.0 | 6.015321884 | 23.42548023 |
| 92.0 | 6.027043100 | 25.16577855 |
| 94.0 | 6.038319489 | 26.91545559 |
| 96.0 | 6.049180042 | 28.67392134 |
| 98.0 | 6.059651025 | 30.44064002 |
| 100.0 | 6.069756320 | 32.21512323 |

Binding occurs when $E_3 < -61.1169$ e.V.

# APPENDIX II

TABLE VII

GOLD ALLOY PARAMETERS AND CALCULATED VALUES

| Impurity | $\Delta Z$ | $\delta/a$ X 100 | $1/\sigma$ | $1/\sigma$ cal. | N | N cal. | $\delta(\Delta E)$ |
|---|---|---|---|---|---|---|---|
| Ca | 1 | -0.10 | | | 2.24 | | |
| Sc | 2 | 0.0855 | 9.5 | | 1.83 | | 0.0751 |
| Ti | 3 | -0.0259 | 12.9 | 13.00 | 3.06 | 3.09 | 0.0802 |
| V | 4 | -0.0298 | 13.8 | 13.42 | 4.07 | 4.00 | 0.0684 |
| Cr | 5 | -0.0548 | 13.1 | 13.15 | 5.13 | 5.15 | 0.0493 |
| Mn | 6 | -0.0178 | 12.8 | 12.85 | 6.04 | 6.07 | 0.0428 |
| Fe | 7 | -0.0662 | 12.0 | 11.98 | 7.16 | 7.16 | 0.0447 |
| Co | 8 | -0.0841 | 7.1 | | 8.20 | 8.26 | 0.0526 |
| Ni | 9 | -0.0731 | 3.0 | | 9.18 | 9.18 | 0.0430 |
| Cu | 0 | -0.0927 | 0.48 | 0.44 | 0.23 | 0.24 | 0.0350 |
| Zn | 1 | -0.0460 | 0.95 | 0.95 | 1.11 | 1.12 | 0.0373 |
| Ga | 2 | -0.0144 | 2.2 | 2.18 | 2.04 | 2.03 | 0.0230 |
| Ge | 3 | 0.0185 | 5.2 | 5.22 | 2.96 | 2.97 | 0.0172 |
| As | 4 | | | | 3.86 | | |
| Ag | 0 | -0.0021 | 0.32 | | 0.00 | 0.03 | 0.0208 |
| Cd | 1 | 0.0438 | 0.61 | 0.74 | 0.89 | 0.85 | 0.0285 |
| In | 2 | 0.686 | 1.4 | 1.40 | 1.83 | 1.84 | 0.0261 |
| Sn | 3 | 0.0959 | 3.47 | 3.35 | 2.76 | 2.75 | 0.0167 |
| Sb | 4 | 0.1154 | 6.8 | 6.83 | 3.72 | 3.73 | 0.0200 |

Note: with the additional pure gold parameters of $k_F = 1.20 \times 10^{8} m^{-1} = 5.486$ e.V., $\Omega_{Au} = 1.687 \times 10^{-23} m^3$, Wigner-Seitz radius $= 1.591 \times 10^{-8} m$, nearest neighbor distance $= 2.878 \times 10^{-8} m$, and the well-boundary (= 0.5 times the nearest distance) $= 1.439 \times 10^{-8} m$.

TABLE VIII

PHASE SHIFTS, ENERGIES, AND CHARGE DENSITIES FOR THE ALLOYS

| Imp. | $\delta_0$ | $E_0$ | $\delta_1$ | $E_1$ | $\delta_2$ | $E_2$ | $\frac{\langle\Delta\rho\rangle_s}{\rho_{Au}}$* | $\frac{\langle\Delta\rho\rangle_p}{\rho_{Au}}$* | $\frac{\langle\Delta\rho\rangle_d}{\rho_{Au}}$* | $\frac{\langle\Delta\rho\rangle_{tot}}{\rho_{Au}}$[1] | $\frac{\langle\Delta\rho\rangle_{tot}}{\rho_{Au}}$[2] |
|---|---|---|---|---|---|---|---|---|---|---|---|
| Ca | | | | | | | | | | | |
| Sc | | | | | | | | | | | |
| Ti | 1.30 | -10.50 | 0.0 | 0.00 | 0.71 | -25.06 | -0.00020 | 0.0 | 0.01122 | 0.01102 | 0.00935 |
| V | 3.6 | -39.66 | -0.29 | 14.73 | 0.71 | -25.06 | -0.00215 | -0.00228 | 0.01122 | 0.00679 | 0.00776 |
| Cr | -0.188 | | 1.29 | -11.91 | 0.88 | -25.84 | 0.00079 | -0.00808 | 0.01245 | 0.00516 | 0.00474 |
| Mn | 0.34 | -1.92 | 1.23 | -11.55 | 1.10 | -26.61 | -0.00127 | -0.00738 | 0.01330 | 0.00465 | 0.00489 |
| Fe | 1.04 | -7.01 | 1.25 | -11.67 | 1.29 | -27.16 | -0.00140 | -0.00760 | 0.01352 | 0.00452 | 0.00387 |
| Co | 0.22 | -1.19 | -0.35 | 22.67 | | | -0.00087 | -0.00302 | | | 0.00440 |
| Ni | -0.54 | 3.92 | -0.14 | 4.82 | | | 0.00232 | -0.00086 | | | 0.00348 |
| Cu | -0.06 | 4.54 | -0.06 | 1.51 | 0.12 | -15.50 | 0.00026 | -0.00025 | 0.00294 | 0.00295 | 0.00197 |
| Zn | 0.34 | -1.93 | 0.10 | -2.21 | 0.22 | -19.33 | -0.00127 | 0.00034 | 0.00491 | 0.00398 | 0.00347 |
| Ga | 0.93 | -5.95 | 0.34 | -5.36 | 0.25 | -20.06 | -0.00173 | 0.00033 | 0.00547 | 0.00407 | 0.00250 |
| Ge | 1.75 | -20.76 | 0.50 | -6.94 | 0.28 | -20.69 | -0.00230 | -0.00034 | 0.00598 | 0.00334 | 0.00263 |
| As | | | | | | | | | | | |
| Ag | -0.225 | 1.40 | -0.05 | 1.40 | 0.08 | -12.60 | 0.00097 | -0.00020 | 0.00208 | 0.00285 | 0.00255 |
| Cd | -0.042 | -0.24 | 0.11 | -2.30 | 0.21 | -18.92 | 0.00020 | 0.00034 | 0.00472 | 0.00526 | 0.00470 |
| In | 0.45 | -2.58 | 0.28 | -4.76 | 0.32 | -21.44 | -0.00158 | 0.00044 | 0.00664 | 0.00550 | 0.00503 |
| Sn | 1.26 | -9.76 | 0.57 | -7.47 | 0.27 | -20.58 | -0.00044 | -0.00073 | 0.00580 | 0.00463 | 0.00457 |
| Sb | 1.94 | -25.11 | 0.86 | -9.36 | 0.27 | -20.52 | 0.00282 | -0.00312 | 0.00580 | 0.00550 | 0.00548 |

*Values obtained from generated scattered charge density curves; [1]sum of the previous three columns; [2]value obtained directly from the differential Mössbauer isomer shift via Table I and Equation III-3.

# VITA

Trent Lee Nichols, son of Ted and Audrey Nichols, was born on 4 April 1954 in Knoxville, Tennessee. He attended Spring Hill Elementary School in that city and was graduated from Holston High School in June of 1972. The following summer he entered The University of Tennessee, and in June 1976 he received a Bachelor of Science degree in Engineering Physics with honors. In the fall of 1976 he accepted a graduate assistantship at The University of Tennessee in the Physics Department and began study that fall toward a Master of Science degree. This degree was awarded in December 1978.

The author is a member of American Physical Society, American Association for the Advancement of Science, Society of Physics Students, and Sigma Pi Sigma. He is currently the president of The University of Tennessee chapter of Sigma Pi Sigma and has served as vice-president and secretary of the same organization. Mr. Nichols will be pursuing a Doctor of Philosophy degree at The University of Tennessee beginning in the winter of 1978.

He is married to the former Sally Ann Summers of Memphis, Tennessee.